Mechanical Characterisation for Simplified Response Modelling of Woven Polypropylene

by

David Rostin Ellis

Thesis presented in partial fulfilment of the requirements for the degree of Master of Engineering (Mechanical) in the Faculty of Engineering at Stellenbosch University

Supervisors: Dr. M.P. Venter
Prof. G. Venter

March 2017

Declaration

By submitting this thesis electronically, I declare that the entirety of the work contained therein is my own, original work, that I am the sole author thereof (save to the extent explicitly otherwise stated), that reproduction and publication thereof by Stellenbosch University will not infringe any third party rights and that I have not previously in its entirety or in part submitted it for obtaining any qualification.

Date: March 2017

Abstract

Mechanical Characterisation for Simplified Response Modelling of Woven Polypropylene

D.R. Ellis

Thesis: MEng (Mech)

March 2017

Methods of modelling woven polymer textiles within the Finite Element (FE) environment result in a compromise between level of detail captured, computational resources required and simplicity in its implementation. This research has attempted to develop a methodology that simplifies this process starting from the physical mechanical testing of the material.

A biaxial and shear test rig was developed capable of testing for material response at various biaxial load ratios. Tests were performed at the fabric level using a single cycle load path to the maximum desired load before gradually being reduced to zero whilst the material deformation was captured using Digital Image Correlation. Time-dependent material response was not tested for specifically.

The response of the material was calculated as the instantaneous stiffness and modelled as a function of strain using a combination of power law and linear regression fits. An equation was derived that allows for the unload response to be modelled using data for a full-load test, but be applied to loads intermediate thereof, all whilst being implementable within the FE environment. This material law was implemented as a user-defined subroutine for MSC.Marc as demonstration of its intended use and application. The methodology proved accurate at determining the load and unload paths for loads intermediate to those physically tested for.

Uittreksel

Meganiese Karakterisering vir Vereenvoudigde Gedrag Modelleering van Geweefde Polypropeleen

D.R. Ellis

Tesis: MIng (Meg)

Maart 2017

Metodes om geweefde polimeer-tekstiele te modeleer binne die Eindige Element (EE) omgewing is grotendeels 'n kompromie tussen die breedvoerigheid van die besonderhede wat vasgelê kan word, die vereiste rekenaarberekeningsvermoë en die moeilikheidsgraad wat gepaard gaan met die implementering daarvan. Hierdie navorsing het gepoog om 'n metode te ontwikkel wat die proses vereenvoudig vanaf die fisies-meganiese toetsproses.

'n Biaksiale skuifwerking-toetstuig met die vermoë om materiaal-reaksies by verskeie biaksiale ladingsverhoudings te meet is ontwikkel. Toetse is op materiaalvlak uitgevoer deur middel van 'n enkel-siklus ladingspad tot by die maksimum gewenste lading, waarna die lading geleidelik verminder is tot nul en die materiaal-vervorming tegelykertyd vasgevang is met gebruik van Digitale Beeld Korrelasie. Daar is nie spesifiek getoets vir tyd-afhanklike materiaalreaksie nie.

Materiaal-reaksie is bereken as oombliklike styfheid en gemodelleer as 'n funksie van vervorming met behulp van 'n kombinasie van logaritmiese en lineêre funksiepassings. 'n Vergelyking is afgelei wat dit moontlik maak om die materiaal-reaksie te modelleer soos dit vervorm vanaf die maksimum aangewende krag terug na nul, gegewe die data vir 'n vol-las siklus, maar toegepas op intermedieêre-las aangeleenthede. Hierdie vergelyking is van toepassing in die EE omgewing. Materiaal-reaskie is as 'n subroetine geïmplementeer in

MSC.Marc om die uiteindelike toepassing en gebruik daarvan te demonstreer. Die metode is getoets en as akuraat bevind om die volle siklus van materiaal vervorming vir intermedieêre lasprofiele te bepaal.

Acknowledgements

A special word of thanks to the following people who contributed to the completion of this project:

Andre and Dianne for their loving support throughout the years.

Michael and Sonja for being a home away from home.

The departmental workshop staff for their willingness to discuss ideas and sharing of practical knowledge gained over countless years.

Doctor Martin Venter for being a very accessible supervisor and always making one question the norm.

Professor Gerhard Venter for his wealth of knowledge in not only the field, but also in guiding students.

Vortex Innovation Worx Pty Ltd for project funding.

Table of Contents

List of Figures

List of Tables

Chapter 1

Introduction and Project Outline

The ability to accurately predict the mechanical behaviour of woven textile polymer materials through mathematical modelling is a difficult topic (Hu, 2004). This technological problem is seen as a limiting factor in the application of numerical models to prototype structural applications of these materials. The main focus of this study is to characterise the mechanical response of an uncoated polymer material such that a model thereof can be included in a nonlinear finite element analysis. This chapter gives an overview of the project as a whole; background information is provided and the position where it fits in with respect to ongoing research is outlined. The research objectives are stated and explained. Important previous research done is highlighted sufficiently to make the objectives clearer, but a thorough investigation thereof is left for the succeeding chapter.

1.1 Background and Motivations

Dunnage bags are pillow-shaped bags used to secure goods during transportation. This is achieved by inserting the flat deflated bag into a void and subsequently inflating it with air to fill the void and prevent the possibility of damage caused by the movement of goods. Research into the development of a virtual numerical inflatable dunnage bag model utilising an uncoated plain woven polypropylene cover as reinforcement by Venter (2015) brought to light the lack of a robust and practical means of modelling the woven material within the

finite element environment. The numerical model, constructed using explicit nonlinear finite element methods, was required for research and development purposes with the overall objective of gaining a better understanding of their response during working conditions. Large forces subjected over extended time periods and dynamic loading cycles constitute typical loading scenarios.

The accuracy of numerical models depend on, amongst other factors, representative material properties and modelling. Analysis tools for efficient design involving woven materials lag behind those for conventional materials. Changes in fabric architecture occur with loading and lead to several sources of nonlinear responses. The requirement of accurate material data and models capable of effectively matching the material response within a finite element analysis were key components of the study and required extensive research. Various methods of modelling the material were adapted to be suitable for application to dunnage bags. These methods varied in complexity and application generality and yielded satisfactory results for the scenario under consideration. However, higher accuracy and the possibility of application to a broader spectrum of structures are required from the material model before structural optimisation can be undertaken. Known phenomena that play a role in the modelling of the material needed to be explored further.

At working inflation pressure, inflatable structures are loaded well within the plastic region of the material. Dynamic loading also occurs which further increases the extent of plasticity experienced. This recurrent loading requires that the material be described not only during loading thereof, but also during unloading. Further, the nature of woven textiles is such that the interactions between yarns largely dictate the response of the material. Constructing numerical models that incorporate a level of detail fine enough to capture such interactions has proved troublesome due to computational restrictions (Parsons *et al.*, 2010). The most important aspect of modelling is creating models that can produce accurate results for different loading conditions. Modelling, and simulation in general, is performed to extract key information that would not be available from physical experimentation alone.

Woven polymer textiles are increasingly being used in structural applications not necessarily related to inflatable structures. The loading mechanisms between inflatable and purely structural applications are largely similar and therefore allow the same methodology to be used for their characterisation

and numerical modelling. Further, variability in material strength between textile polymers intended for a similar application leads to a result where it is more attractive being able to easily generate a material model using minimal physical testing. Material models that fully characterise the response for numerical implementation, but require the use of specialised testing equipment, are undesired as such an approach could require the use of published properties gathered from extensive material testing.

1.2 Project Scope and Objectives

This thesis sets out to meet three objectives, each identified as milestones along the road of meeting the overall research goal of improving the methodology for testing and modelling woven polypropylene. All three of these objectives are stated below and a brief argument provided, justifying their individual importance.

1.2.1 Experimental Test Procedure

The existence of a credible and comprehensive set of test data from material response measurements is paramount to the success of mechanical characterisation of any material. The first objective is to create a methodology for physical testing and ensuring that it can be adhered to by procuring the relevant systems. This involves establishing the applicability of equipment currently available and using that information to guide the design process of new system components. Accommodating time-dependent material behaviour during physical testing falls outside the scope of this project and is left as a recommendation for further research. The increased complexity can be added once an interim solution to the overall research objective has been found.

1.2.2 Response Modelling

A study of the experimental results needs to be conducted to decide the method whereby the response will be modelled. The extent to which the material response needs to be modelled depends on the material modelling approach used. Certain approaches require a data set used merely to calibrate the engineering parameters of the specific model (which can take place within most

commercial FE software packages), where other methods attempt to directly model the response and use that to form a regression or statistical model for further use. This objective attempts to capture all the known behavioural characteristics of the material within the scope of the project.

1.2.3 Numerical Implementation

Different material modelling approaches have different extents to which numerical implementation is required. Calibrating a material model available within the FE software package requires no implementation, whereas creating a new model will require extensive implementation effort. The nature of the material does not lend itself, for the time being, to be represented using already implemented material models. This leads to the requirement of creating a user-defined subroutine being able to run in parallel with an FE analysis. The completion of this objective should culminate with a working material modelling approach implemented in MSC.Marc.

1.3 Thesis Outline

The different concepts and theories of this thesis are discussed before progression to application of the knowledge. In Chapter 2 the material is explained from a material mechanics point-of-view, different considerations are given for numerical modelling thereof, and literature consulted for physical test rigs. Chapter 3 details the design and commissioning of the manufactured biaxial test rig. Material response results for various load cases as well as the test procedure followed are explained in Chapter 4. The modelling of the material response and the subsequent numerical implementation thereof is detailed in Chapter 5 with Chapter 6 presenting the methodology validation. Final conclusions regarding the initial aim and objectives are presented in Chapter 7 with recommendations being proposed for future work.

Chapter 2

Polymer Textile Testing and Modelling

Solid polymer materials have a number of interesting responses to mechanical loading (Bergstrom, 1999). In addition, the response of textile variations thereof differ considerably from their continuous counterparts. They are heterogeneous, noncontinuous and have anisotropic behaviour; they are easily deformed, suffering large strains and displacements and exhibits plasticity and nonlinear behaviour even at low stresses and room temperature (Hu, 2004). It is known that for woven textiles the material response is based not only on the material properties of the base material, but also on the mechanics of the weave architecture and kinematics (Cavallaro *et al.*, 2003).

2.1 Textile Architecture and Manufacturing

At their lowest level textiles are constructed of individual fibres of which many grouped together constitute an individual tow which ultimately are woven to construct the material at the fabric level. A plain woven polypropylene material used as reinforcing cover for a high-strength, premium quality dunnage bag is used as candidate material for characterisation. These bags are used to restrain heavier loads and are constructed from a noticeably stiffer material. A close-up of the weave architecture is shown in Figure 2.1. In this weave pattern every individual tow fed from the machine direction (MD) is laced orthogonally with a tow fed from the cross direction (CD) in an over-and-under alternating configuration. Textile terminology refers to these material direc-

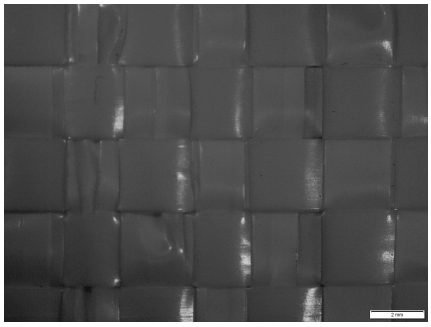

Figure 2.1: Plain weave architecture as viewed under a microscope (Magnification: 8x)

tions as warp and weft directions, respectively. The locations at which tows overlap are called the crossover-points.

It is possible to employ different tows of varying size and materials to change the mechanical properties of the textile as a whole. Individual tows are pre-stretched prior to the weaving process to increase their stiffness and reduce their elongation to break (Venter, 2015). The degree of pre-stretch differs between these orthogonal tows. Further, a double tow design in the warp direction and a single tow in the weft direction is utilised. These dissimilar properties result in an unbalanced weave, whereas textiles attempting to match the properties in the two material directions are classified as being balanced (Tan *et al.*, 1997).

2.2 Mechanical Response of Textiles

The mechanical behaviour of even relatively simple plain woven fabrics is complex due to the intricate interactions of the yarns that constitute the fabric mesostructure. Plain woven fabrics appear to constitute an orthotropic response, but its behaviour is uncharacteristic of that for a continuum material. The fabric rather behaves as a discrete assemblage of individual tows whose effective properties are dependent on weave geometry and material loading (Cavallaro *et al.*, 2003). King and Socrate (2004) performed a series of tests on fabrics of varying weave densities. They found that material response was significantly affected by tow kinematics at the cross-over points and initial fabric geometry. King *et al.* (2005) investigated the mechanical response of woven fabrics in detail. They found three different tow interactions that result in varying responses:

- **Crimp interchange** – The interaction between perpendicular tows of a material being loaded and the subsequent transfer of crimp content between these directions.
- **Locking** – A mechanism by which the fabric geometry resists further deformations as the interwoven tows jam against each other.
- **Resistance to relative yarn rotation** – The dominant mechanism for the response of fabric to in-plane shear.

The criss-crossing nature of tows relative to each other as a consequence of the weaving process results in tows approximating a wave-like shape. A tow extracted from the candidate material, as viewed from the side under a microscope, exemplifies the occurrence in Figure 2.2. The extent of crimp is quantified by the crimp content, C, defined by Hearle *et al.* (1969) using two orthogonal material directions and a plain weave as $C = L/P - 1$, where L is a reference length along the tow in the direction that the crimp content is desired, and P the tow spacing frequency. Crimp is therefore measured as the ratio of the difference between the straightened and as-woven tow length to the as-woven tow length. Upon uniaxial loading, the tows in the loaded direction will straighten, or decrimp, causing the subsequent apparent shortening of the tows normal thereto as crimp is transferred between the material directions. This crimp interchange can occur without any elongation of tows and is primarily driven by geometry. This coupled response between material directions is illustrated in Figure 2.3 as a side-view of the material architecture. The as-woven material in Figure 2.3a is tensioned in the warp direction, leading to the straightening thereof and shifting of weft tows further apart, evident in Figure 2.3b. Cavallaro *et al.* (2007) note that the force-displacement response of uncoated fabrics to biaxial tension is dominated by crimp interchange, resulting in a three-dimensional state of deformation.

Rotation of tows relative to their original directions when the material is biaxially loaded and subjected to an in-plane rotational stress constitutes the load scenario required for shear response. As with tensile response, shear response is primarily dependant on textile kinematics, and as such is a system property as opposed to a quantifiable material property (Cavallaro *et al.*, 2003). Further, the non-continuous material decouples the relationship between shear

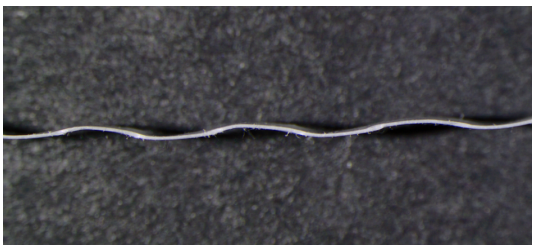

Figure 2.2: Individual warp tow as viewed from the side under a microscope (Magnification: 8x)

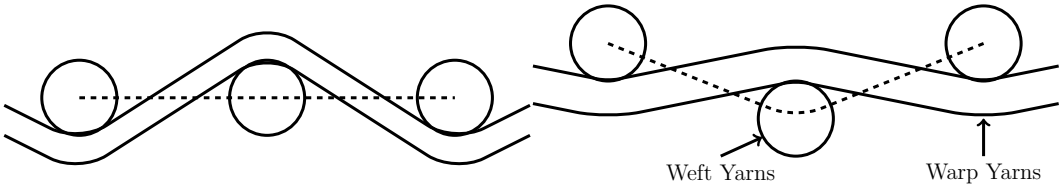

(a) As-woven material

(b) Decrimped material

Figure 2.3: Illustration of crimp interchange

and elastic modulus. The three distinct stages of shear deformation, illustrated in Figure 2.4, were identified by Farboodmanesh *et al.* (2006) as:

- **Initial state** – As-woven material prior to shear loading.
- **Shearing/Compaction** – Initial friction-dominated rotation at the cross-over points requiring low shear loads.
- **Locking angle/Compaction limit** – Increasing fibre volume fraction leads to an increased resistance to shear loading as tows are crushed tightly together.
- **Wrinkling** - Voids in textile geometry do not allow for further tow rotations, resulting in material wrinkling out-of-plane.

The stress-strain behaviour of woven materials under tension is described by Hu (2004). At low stresses the initial tensile stiffness is small due to straightening of crimped yarns. At high stresses when decrimping is nearly complete and inter-fibre friction is increased, the tows are elongating, the fabric structure becomes consolidated and the fibres better oriented. This leads to an almost linear stress-strain relationship, which is similar to conventional metallic engineering materials. In the intermediate range, the consolidation and yarn reorientating process is reflected by the nonlinear stress-strain curve.

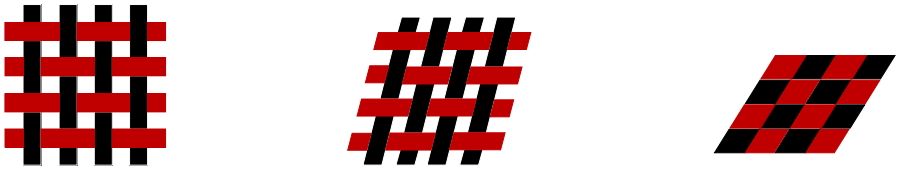

(a) Initial state (b) Shearing/Compaction (c) Compaction limit

Figure 2.4: Shear stages of textiles

Literature on biaxially loaded textiles exists within three clusters, each concerning different applications, identified by Cavallaro *et al.* (2003) as:

- **Textile composites** – Primarily focused on material testing required for simulations of textile forming/draping processes. The effects of internal pressure are not of concern.
- **Structural composites** – The study of in-plane effective elastic properties of composites comprised of polymer fibres and a stiff matrix.
- **Inflated tensile structures** – Material response measuring for applications simulating inflated structures. Material response is generally homogenised for increased computational efficiency.

Forming and draping processes subject textiles to a deformation mode dominated by that of shear without much tensile loading. A collaborative effort by Cao *et al.* (2008) attempted to benchmark the test procedures used by seven research institutions specifically for shear response. Trellis-frame (picture-frame) and biased extension tests were used throughout. They found consistency between institutions. The increase in achievable repeatability of using mechanically pre-conditioned samples was highlighted and the difficulty in calculating well-defined normalised results from inhomogeneous materials established. The lack of tensile response measurements and the identification by Venter (2015) that failure zones in pillow-shaped inflatable structures are in regions not dominated by shear deems this literature cluster of less interest for the current study.

Structural composites are typically used as replacement for conventional metallic materials due to their light weight and high strength. These structures are designed such that loading remains within the linear-elastic range of the

material. The inclusion of the stiff polymer matrix drastically changes their response such that characteristics inherent to non-coated woven textiles cannot be observed. Literature covering the design using such composites offers little to the characterisation of the candidate material.

Research into modelling large inflated structures often comes at the cost of reduced model complexity, rather opting for simpler isotropic models and increased computational efficiency. Physical testing, to this end, has therefore focused on calibrating such models. The load case that these structures are subjected to is not described well in an isotropic manner and further advances in the field are needed to progress past this limitation.

Inflatable structures undergo large out-of-plane displacements from their stowed to deployed shapes; however, loading is primarily in-plane. Under biaxial tension, the tow-tow interactions consist of two components, a pressure independent adhesive component and a dominant pressure-dependent frictional component (Pan, 1996). Deformations resulting from pressurisation are dominated by sliding of the yarns at the crossover points and crimp interchange rather than fabric shearing (Cavallaro *et al.*, 2007). Potluri and Thammandra (2007) pointed out the abundance of literature on shear over that of tensile.

2.3 Numerical Modelling Strategies

Modelling of textiles for numerical implementation can be undertaken using fundamentally different approaches incorporating varying levels of detail. Hu (2004) identifies the three approaches as:

- **Component–orientated** – This starts with physical concepts and assumptions which are used to facilitate further deductions. The theoretical basis hereof is Newton's third law, minimum energy principles and mathematical analysis of construction. The combination of yarn properties, inter-yarn interaction and fabric structures is used to predict mechanical responses.

- **Phenomena–oriented** – Rheological models incorporating components such as springs and dashpots are constructed capable of matching the response to applied loads. These components are selected to model re-

sponses such as elastic, plastic, viscoelastic and frictional effects as observable in results from physical testing.

- **Results–orientated** – A hypothesis is formulated to describe experimental results whereafter the relationship of the function with fabric components is sought. The theoretical background of this approach is concerned with pure mathematics and numerical methods. However, this approach allows estimates to be made of purely mathematical operations, thus avoiding misleading subjective assumptions. As the analysis proceeds, more complex phenomena may be uncovered which can be used to refine the approach.

The specific chosen approach to modelling does not stipulate the level of detail incorporated in the model. This is determined by the level of detail required from the simulated model. Lomov *et al.* (2001) gives the hierarchy of textile modelling strategies as:

- Fibre → Yarn/Tow
- Yarn/Tow → Fabric weave
- Fabric weave → Unit cell of part
- Unit cell → Complete part

For inflatable structures where there is a significant difference in the order of magnitude between the structure and the individual tows that constitute it, modelling the textile on a fibre basis becomes impractical due to computational restraints. Appropriate simplifications can be made in order to conduct modelling from a continuum mechanics approach, but has the drawback that yarn interactions cannot be captured (Parsons *et al.*, 2010).

2.4 Woven Textile Modelling

In practice, the most popular material modelling technique is the development of mathematical models based on the observation of material behaviour during experimental testing and a list of assumptions and simplifications. Thereafter, the mathematical model is postulated to give a qualitative explanation of the

observed behaviour. Behaviour such as elasticity, plasticity, creep, etc. as noted specific to the material under consideration can all be accounted for in the mathematical model. This process is often assisted by the use of different rheological elements created to model certain behaviour. These rheological models consist of a network of springs and dash-pots connected in series and parallel to achieve the desired outcome. Calibrating these models requires tuning the various elements' parameters. This method achieves good accuracy with most metallic materials and has successfully been used for solid polymers (Bergstrom, 1999). Essentially, for this research, it is desired that the intricate interactions of the deforming textile can be accounted for by a model that disregards the mechanics thereof, but rather models the homogenised response over a larger area. The coupled tensile behaviour between the orthogonal material directions, non-linearity during biaxial loading and unloading, and the significant plasticity are the important material characteristics that need to be captured. Known effects such as strain-rate dependence and severe creep at room temperature do not fall within the scope of this research. Time-dependent material characteristics are included in a discussion regarding future work. Various homogenisation approaches have been devised in literature for modelling woven textiles, identified by Venter (2015) as: meso-scale models, parameter identification through unit-cells, and material response matching.

2.4.1 Meso-Scale Modelling

Meso-scale modelling fits between micro- and macro-scale/fabric-level modelling. It is a powerful technique for homogenisation of mechanical properties at the tow level. Yarn interactions are taken into account by modelling each yarn individually using an appropriate geometrical shape. The fibres constituting each yarn are, however, not modelled and therefore the yarn is considered as continuous. The achievable detail requires significant computational resources and is therefore often an impractical method of modelling. Lomov *et al.* (2007) created a comprehensive road map to follow for the development of meso-scale models based on their experience with various textiles.

Ivanov *et al.* (2009) specifically researched the validity of meso-scale FE models. They identified numerous factors within the geometrical and mechanical modelling as well as in the numerical algorithms potentially being sources of error. Digital Image Correlation (DIC) was used to measure strain

on a physical sample. It was found that a very high resolution is required for measurements. The two models showed that it is difficult to achieve close correlation on a meso-scale.

Sagar *et al.* (2003) made use of the energy method to meso-scale model the interlaced fibre assemblies. Their model incorporated the nonlinear properties of the constituent yarns, rather than a simplified linear behaviour thereof as used during other studies. The possible deformation mechanisms playing a role were identified as yarn elongation, bending and compression. Provision for the inclusion thereof was made. The conventional geometrical yarn path from Peirce (1937) was adapted to a polynomial path for ease of parameter evaluation and more accurate representation of a real weave. The result was a computationally efficient algorithm capable of accurately modelling load-deformation behaviour.

The practicality of meso-scale models was brought under question by Cavallaro *et al.* (2003). The contact surfaces between tows were shown to produce convergence issues in solving their numerical model. Further, the greatly extended time required for solving such models further jeopardizes its practicality. The level of detail captured in meso-scale modelling is high and the computational resources required therefore considerable. The result would thus be that detail is captured which, when considering the full size structure, is largely irrelevant.

2.4.2 Unit-Cells

Unit-cells represent a homogenisation technique used to simplify complex geometries to those that can be described using fewer parameters. By analysing the smallest geometrical repetitive unit it is possible to achieve properties representative of the material. This is done in an attempt to reduce the number of finite elements required in a numerical analysis from the excessive amount used for meso-scale modelling down to a lower quantity. Elements in the unit cell are chosen such that some of the yarn interaction is preserved, while run-time is reduced. The response of these cells is used to characterise the material properties of the structure being investigated. Two different approaches to unit-cells exist: numerical and analytical. Analytical models are often less complex due to simplifying assumptions, but lead to restrictive model generality. Numerical unit-cells can better describe the 3-D interactions within the

structure; however, higher modelling effort and custom numerical discretisation for individual fabric architectures are required (Adumitroaie and Barbero, 2011). Both of these approaches rely heavily on accurate boundary condition representation. This representation often forms the main focus of new unit cell derivations.

Numerical Unit-Cells

Numerical unit-cells are often constructed from a representative section of the textile incorporating the appropriate level of detail concerning its architecture, by modelling the section using solid finite elements. The process of developing this meso-scale FE model was simplified by Verpoest and Lomov (2005) by developing the software *WiseTex* which implements generalised descriptions of internal structure for various architectures.

A plain weave architecture was modelled by Peng and Cao (2002) at the meso-scale whereafter the characteristic pattern thereof was encompassed in a unit-cell. They found that the nonlinear response could be accounted for accurately using this approach. Their model, however, focused on determining the nonlinear effective elastic moduli and therefore cannot capture permanent plastic deformations.

Grujicic *et al.* (2009) also investigated a meso-scale unit-cell based material model of flexible fabric armour for use as a user-defined subroutine in commercial FE software. Their main intent was to attain computational efficiency while not significantly sacrificing physical characteristics of the fabric architecture and behaviour. The meso-scale model of the weave was represented as two yarns constructed with 8-node hexahedron finite elements and the response thereof matched in a numerical unit-cell. This user-defined model could reasonably well account for the damage sustained during impact of a projectile. Lin *et al.* (2008) also developed a unit cell discretised using tetrahedral elements, but implemented constitutive yarn models describing the yarn behaviour accurately, instead of a transversely isotropic description. This method proved computationally less costly than conventional meso-scale modelling alone.

Shahkarami and Vaziri (2007) developed a shell-based meso-mechanical model for capturing essential components of plain woven textiles, including dynamic effects. Their approach used a 3-D unit cell which provided a baseline mechanical response for calibrating the analytical constitutive model in an

equivalent orthotropic shell element representation. This model was validated using impact simulations and proved to be an efficient technique capable of accounting for detailed geometrical and material properties.

A similar approach was used by Peng and Cao (2005) to create a representative shell element replicating the mechanical response of a unit cell. A non-orthogonal constitutive model was developed with the assumption of decoupling the shear-tensile response and tensile response between warp and weft directions. The aim was to capture the anisotropic material behaviour caused by complex fibre reorientation. The decoupling required that only shear and uniaxial material tests be performed, thereby making redundant the use of equipment capable of biaxial tensile testing. Liu *et al.* (2005) went a step further and tried to eliminate the need for fabric-level experimental characterisation by proposing an analytical solid mechanics model to predict the shear properties of woven fabrics. A proper prediction of the frictional resistance however inhibited the model from being complete.

While investigating the effect of inflation pressure in inflatable structures on elastic and shear moduli, Cavallaro *et al.* (2003) developed a beam element unit-cell model to characterise the effective constitutive relations. In this model each individual fibre in the tow was accounted for within the representative area using beam elements. These elements proved to be a more realistic representation of the tows. This material representation was then tested during different load cases.

Analytical Unit-Cells

Analytical unit cells aim to a similar outcome as their numerical counterpart, but rather through an analytical means requiring extensive mathematical derivations and constitutive relations. Constitutive relations are the link between an externally applied parameter and the response thereof by the system. A typical constitutive equation is the relationship between applied stress and resulting strain. These relations form part of the backbone of constitutive modelling. Information specific to the material under consideration is added by such relations. These constitutive relations are then used to homogenise the material by modelling it as a planar continuum with preferred material directions. The appeal of this technique lies in the computational efficiency that can be achieved. In practical applications the constitutive relations are

implemented in FE analyses as user-defined subroutines.

Boisse *et al.* (1997) investigated the use of analytical unit cells for simulating the forming process of textiles. A thorough scrutinising of the experimental results of testing material behaviour was undertaken. Through this the absence of shear stiffness, bending stiffness, compressive stiffness and interfibre sliding between normal directions were established. The biaxial nature of the deformation was identified. Finite elements of the woven yarns were made using nonlinear kinematics and applied in analyses. The model calculated accurate strains in the yarns and allowed valuable conclusions to be made with regards to the forming die validity. A drawback of the model is the extensive calibration required.

The non-trivial process of deriving a unit-cell of much reduced size is covered by Li *et al.* (2011). They made use of all available and independent types of geometric symmetries, formulated them in mechanical terms and used those to derive boundary conditions for a unit cell $1/16^{th}$ the size of a standard repetitive full model. Application of this cell is aimed at micromechanical characterisation of woven textiles. The level of detail captured in this model exceeds that required for the current research, placing high demands on computational resources for large structures.

A thorough investigation into the development of a continuum constitutive analytical model was undertaken by King *et al.* (2005) with the process involved being explained in detail. Their approach requires a geometric model for the fabric architecture which is then described using constitutive models of the tow behaviour. This model was implemented in ABAQUS and used to simulate different modes of deformation. Accurate results were calculated by the model during uniaxial tests in the warp, weft and bias directions. A shortcoming of this model, however, is its inability to capture the unload response of the material response, the permanent deformation caused by plasticity and the lack of biaxial tensile test results used in calibration.

2.4.3 Supervised Learning Models

A more modern computational paradigm, known as knowledge-based methods, provides a fundamentally different approach to material modelling. This representation does not need prior assumptions based on behaviour and is trained solely on experimental data instead. This method has gained a resurgence as

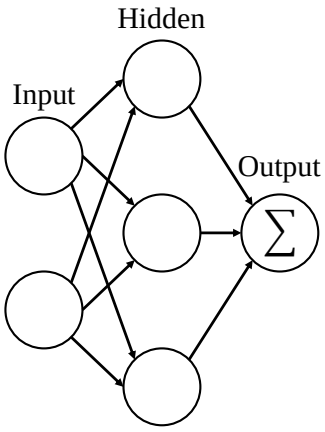

Figure 2.5: Artificial Neural Network

of late driven by increasing computational power and popularity of materials tailored to specific applications which exhibit complex behaviour.

Knowledge-based methods form a subfield of artificial intelligence and evolutionary computing called connectionism where data obtained from experimental testing is used as an example to train a model to perform a specific task. Thus, supervised learning is therefore essentially deducing a function from the training set which can be achieved using either of a selection of algorithms, the most widely used being Support Vector Machines (SVM) and Artificial Neural Networks (ANN).

An ANN is constructed using a multitude of fully interconnected nodes arranged within various layers, inspired by that of a biologically brain. An example of such a network is illustrated in Figure 2.5. These nodes, or neurons, act as processors and are essentially individual weights along with some nonlinear transfer function that relate any number of inputs to outputs, forming a model of the data. These weights assume random starting values and are calibrated using a learning rule and a set of training data. A very basic rule is that of the backward propagation of errors, or backpropagation, where the networks' prediction from input data is compared to the known output of that data. A loss function is calculated where the gradient thereof is used during an optimisation procedure to minimise the loss function by updating the individual nodal weights. This procedure is done in an iterative manner until a sufficient convergence tolerance is met.

As pointed out by Furukawa and Yagawa (1998), ANN based constitutive

models are implicit in nature and can be constructed using only input-output data. It is therefore not required to have explicit expressions of the material behaviour. The practicability of modelling material response with ANN's was investigated by Ghaboussi *et al.* (1991). They demonstrated this ability using biaxial and uniaxial cyclic models of plain concrete. A more detailed study focusing heavily on the material modelling was undertaken by Ghaboussi *et al.* (1999). They state that a network trained on a comprehensive set of stress-strain data would qualify as a material model through the network's generalisation ability to approximate results that it was not necessarily trained on. Supplying sufficient information to characterise path-dependent behaviour was found to be crucial in their studies.

An accurate material response model is but one step in the process of describing a material for numerical implementation. An ANN-based material model does not generate a material stiffness matrix during its formulation. Lefik and Schrefler (2003) and Hashash *et al.* (2004) represented an ANN response model within an FE code using an incremental constitutive law. It was achieved by allowing the FE model to query the material model at element integration points for the updated state of stress. This updated state of stress is used along with the stress-strain relationship to extract the material stiffness matrix. Jung and Ghaboussi (2006) followed a similar approach, but applied it to rate-dependent materials. They found the model capable of describing a visco-elastic material response accurately, but state that the issue of what constitutes a sufficient set of training data has not been resolved.

Modelling hysteretic-like load-unload material response was researched by Ghaboussi *et al.* (1991) and Yun *et al.* (2007). The former was successful in modelling the cyclic behaviour of the uniaxially tested plain concrete by including history information into the network in the form of current and two previous points on the stress-strain curve. They, however, did not demonstrate the ability of the network to predict strains for loads where the exact cyclic path of the training set was not followed. Yun *et al.* (2007) successfully implemented a model capable of capturing hysteretic behaviour into a commercial FE code, ABAQUS. This was achieved by introducing internal variables into the network as:

$$\xi_n = \sigma_{n-1}\varepsilon_{n-1} \ , \qquad \Delta\eta_{\varepsilon,n} = \sigma_{n-1}\Delta\varepsilon_n \tag{2.1}$$

with the subscripts n indicating the n^{th} incremental step. The variable ξ_n is the

previous equilibrium state defined by the energy thereof. The second variable is for the strain control form implying the direction for the next time or load step along the equilibrium path (Yun *et al.*, 2007). They tested the network in recurrent mode where the predicted stresses for one step are used as inputs for the next in order to gauge the robustness in the presence of errors. They found that a comprehensive set of training data was required to represent the material response. The effects of variable load step size for nonlinear analyses required further research.

Neural networks are often complex and the process of deciding on the specific network architecture is a time consuming step that follows a trial-and-error approach. These drawbacks were circumvented by Javadi *et al.* (2009) by using another data-driven method, evolutionary polynomial regression (EPR), to find polynomial structures representing the material response. A genetic algorithm is employed to explore the error surface of the objective function, where criteria can be set to avoid noise in the data and direct the models towards simpler structures. They presented a procedure for determining the material stiffness matrix from the trained EPR model and implemented it in a commercial FE code, ABAQUS. The methodology proposed does, however, require input from the user to select the appropriate objective function based on engineering judgement. Further, the methodology was only tested using the stress-strain curve for a metallic material during loading. The unload prediction capabilities for a material exhibiting a large plastic regime was not demonstrated.

2.5 Non-Contact Displacement Field Measuring

Woven textiles are not suited to conventional methods of strain measurement. Widely used devices such as clip gauge extensometers and foil strain gauges are inadequate for a number of reasons. The attachment of a strain gauge to the surface of a sample affects the local material response. Further, adherence issues stemming from the chemical bonding can be expected related to the high strains experienced by the material. Non-contact methods of measuring the displacement field are preferred for these situations. This practical issue, along with the desire to measure the homogenized material response, are addressed

by one such method, Digital Image Correlation (DIC). DIC is a method in which a series of images is taken of the deforming surface and used to compute the displacement values (LaVision GmbH, 2015). A random contrasting pattern is required for which a correlation between images is sought. Images are divided into subsets used during the correlation algorithm.

The system available to this project was a setup capable of 3D stereo vision surface displacement measurements. The StrainMaster Portable DIC and two VC-Imager E-lite 5 megapixel cameras were used along with the DaVis software by LaVision GmbH (2014) as a complete DIC solution, from data capturing to results processing.

2.6 Mechanical Test Methods

Determining the mechanical behaviour within the operational strain range through experimental testing is a crucial part of characterising a material. Various test apparatus exist for evaluating tensile and shear behaviour of woven textiles, ranging in complexity and capability. The method of material modelling must be determined before a suitable test method can be chosen; meso-scale modelling requires yarn-level material properties, whereas a homogenised modelling approach requires fabric-level properties. These different properties require greatly different testing apparatus. Widely used test procedures as well as purpose-built physical test rigs for fabric-level testing are investigated within this section.

2.6.1 Available Test Procedures

A set of widely accepted tests that can be performed on easily obtainable equipment, such as tensile test frames is available. A run-down of these tests, showing promise to the project, follows.

Uniaxial Tensile Tests

Uniaxial tensile tests apply a load in a single direction to a sample clamped at both ends. It is a simple extension test that can be used to determine the load-elongation response of the material for that specific direction. It is therefore required to test textiles separately in both the MD and CD.

Biaxial Tensile Tests

A biaxial test is essentially two uniaxial tests that are performed concurrently in orthogonal directions on a cruciform sample. This setup allows for determining properties of orthotropic materials using a planar specimen. The through-thickness response cannot be measured using either uniaxial or biaxial tests; however, for inflated tensile structures that material direction offers negligible strength and is often not considered in analyses.

Biased Uniaxial Tensile Test

Biased uniaxial testing is similar to the standard variant, but utilises a sample that is cut at an angle. This allows the MD and CD to be aligned at an angle of 45 deg relative to the direction of load application. The bias test forms a local trellis shear mode in the specimen located within the centre of the deformed specimen. A major drawback of this method is that uncoated woven textiles cannot support this loading and simply fall apart as soon as the test commences. Tows on either ends of the sample are not connected and therefore rely solely on the inter-tow friction of adjacent tows to withstand the load.

Picture Frame Test

The picture frame test loads a cruciform sample in global trellis shear deformation. The fixture clamps the sample on all four sides and allows for the four corners to pivot. The mechanism is inserted into a tensile test rig from where load is applied. The boundary conditions that ensure homogeneity in the sample, however, have the drawback that undesired fibre tensions result. Due to the weaknesses of both test methods, the measured results from the picture frame test and biased uniaxial tensile test are often combined to investigate shear response.

2.6.2 Purpose Built Rigs

Research into mechanical characterisation of textile materials has progressed such that tailor-made test rigs are often required to perform a comprehensive test regime. Two rigs with favourable capabilities are covered.

Cavallaro Rig

Utilising a standard tension-torsion machine, Cavallaro *et al.* (2007) designed and patented a multi-axial tension and shear fixture that consists of various linkages, shown in Figure 2.6. The shear loading is applied to a biaxially preloaded sample by in-plane rotation of one of the directions relative to the other. A clear insight to the effect of pretension on shear response and the effect of biaxial load ratio was found during their research. The camera used for the non-contact optical method of surface strain measurement is situated in the centre of the fixture, directly above the material sample. Load is applied in the vertical direction by means of the tensile testing machine. This load is transferred to the sample via the outward movement of the link members. Adjusting the biaxial load ratio is not a trivial task with this setup.

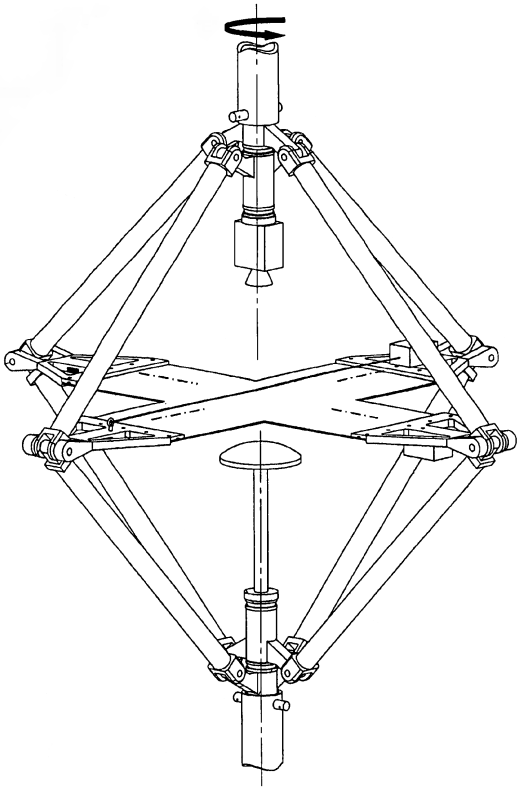

Figure 2.6: Combined biaxial tension and in-plane shear fixture showing the material sample placed horizontally in the centre, the links that transfer the vertical load application to that of a biaxial nature and the video camera required for surface strain measurement. (Cavallaro *et al.*, 2007)

Shear Ramp (Galliot Rig)

The test rig shown in Figure 2.7 is an adapted variant of existing planar biaxial rigs utilising unique load application, developed and tested by Galliot and Luchsinger (2010*a*) and Galliot and Luchsinger (2010*b*). Their proposed method was developed specifically for testing the difficult-to-determine shear response. The use of five independently controlled electromechanical actuators gripping each of the four sides of a cruciform specimen allows for the mitigation of conventional shear testing drawbacks by introducing the shear stress in a pre-stressed sample by means of a shear ramp. An added feature of using independently controlled actuators is the ability to test at various load ratios between orthogonal directions via a simple adjustment on the GUI. The material used during this study utilised a continuous coating allowing for the use of needle extensometers. These were placed in the centre of the material in a triangular configuration. These extensometers cannot be used for measuring deformation of uncoated materials as the opening and closing of voids between tows will lead to displacement errors.

The geometry of the required sample measures 1 m square. This leads to a test rig with a prohibitively large physical size that requires the use of high force electromechanical actuators and large amounts of available material to test.

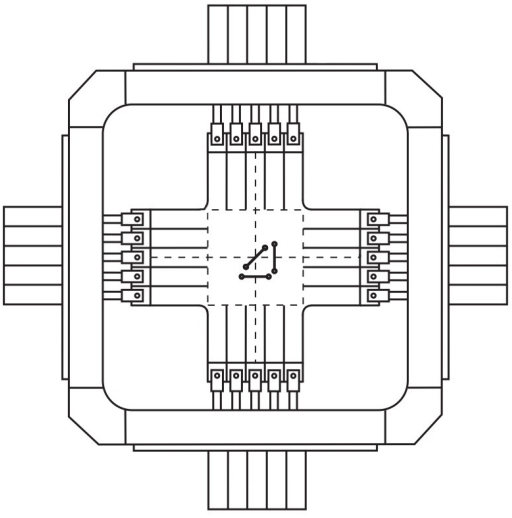

Figure 2.7: Shear ramp test rig showing twenty electromechanical actuators used for load application, the material sample inserted in the centre along with three needle extensometers. (Galliot and Luchsinger, 2010*b*)

2.7 Conclusions from Literature

Considerations that need to be taken for the testing and subsequent numerical modelling of woven polymer textiles were investigated within this section. The architecture of woven materials is such that it can be broken into tangible pieces down to the micro-scale; the fibres which constitute the material. This leads to a large scale difference between the lowest possible section that can be modelled and the eventual intended application to large structures. A wide range of methods to deal with this predicament was investigated.

2.7.1 Numerical Modelling

The numerical modelling methods presented within this section covered a large variety of approaches. The applicability of the models incorporating a high amount of detail make them infeasible for the presented study. By taking into account only the measured response of the material, supervised learning methods follow the desired approach. However, the complexity of these models far exceeds that necessarily required for modelling material response. An alternative and simpler results-orientated approach is sought for response modelling.

In general, the majority of models focus on the loading response of the woven materials and disregard the response during unloading. A method of incorporating the unload response is sought. The method presented for testing and numerical modelling of the material is one where the response is homogenised over a large area relative to the individual tow size. This method enforces a continuum assumption on the modelling, ultimately allowing conventional FE approaches to be used.

2.7.2 Physical Testing

A numerical modelling approach that implements the material response at the fabric-level requires a test rig that can conduct physical testing at that level. The available test procedures are limited to the load cases that can be applied. Biaxial loading and effects of crimp interchange cannot be investigated using those methods. The cost implications linked to the purpose-built rigs are prohibitive to their use during this study. Both of those rigs however show

favourable characteristics; the in-plane application of shear in the rig of Cavallaro *et al.* (2007) and the method of biaxial tension testing in Galliot and Luchsinger (2010*a*). These features were used during the design of a test rig presented in this thesis.

Chapter 3

Design and Commissioning of Physical Test Rig

Establishing material response to mechanical loading with high accuracy and acceptable repeatability requires a proper means of measurement and testing. This criteria gave rise to the development of the aptly named Biaxial and Shear Rig (BASR). Existing test setups were investigated in Chapter 2 and the limitations thereof identified. These limitations were used as the backbone for the design of the presented rig. Key design aspects of this rig are covered and the commissioning phase thereof documented.

3.1 Design Criteria

Geometric limitations of standard tensile test rigs available to the project would jeopardize the functionality of a fixture designed to be used in conjunction with them. The cost-implicated decision was made for an independent, standalone rig. The presented rig was designed to perform biaxial tensile testing not only for use in this project, but rather to become an asset in further materials characterisation research. The key design points were:

- Fabric-level testing on a cruciform material sample with a central region of interest measuring 100 mm square
- Perform biaxial tensile loading up to a maximum of 12 kN for various load ratios

- Ability of in-plane shear application to a minimum of 15° relative rotation
- Ease of repeatable specimen set up to reduce loading time to below 5 min per sample
- An unobstructed and clear view of the deforming samples central region of interest for the DIC equipment

3.2 Final Design

The final design consists of the five main sub-assemblies shown in Figure 3.1. These assemblies perform the different tasks required to meet the design requirements. Further detailed analysis thereof is provided below.

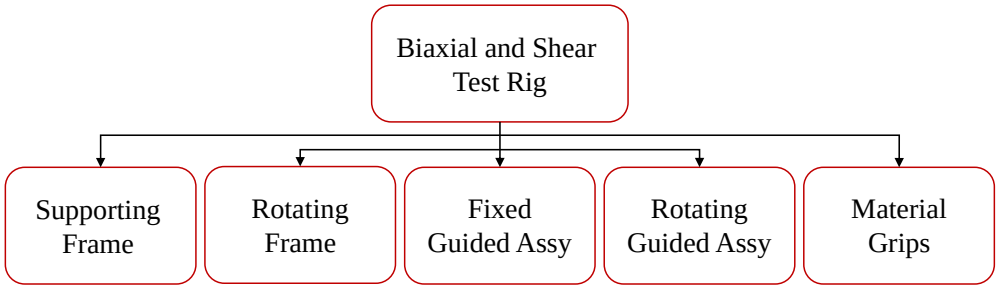

Figure 3.1: Five main sub-assemblies of presented design

3.2.1 Overview

The standalone frame is the structure that supports all of the other components. Its design does not limit the rig to the type of material grips being used or the means of load actuation; both these elements can be changed with minimal effort if certain geometrical limitations are not exceeded.

Load Application

It is required that three distinct loads can be applied to the cruciform sample: one for each of the biaxial directions and a third for the shear loading.

The preferred option of using electromechanical cylinders with electronic drive units for linear actuation was not feasible. It was found that the units

with a high degree of controllability came at an increased cost, whereas the cheaper units lacked the required range of actuation speeds. Instead, a workable and affordable solution was found in pneumatic cylinders. Using four compact high force and short stroke pneumatic cylinders along with two proportional pneumatic pressure regulators would allow for independent load control for each of the biaxial directions. The set of cylinders for each biaxial direction is controlled using a communal regulator. Festo ADN pneumatic cylinders with a piston diameter of 125 mm and stroke length of 80 mm were chosen. At the allowable working pressure of 10 bar these cylinders can exert a force in excess of 12 kN. Festo MPPES regulators capable of maintaining a setpoint pressure accurately were procured.

Rotational loading required for the shear application is achieved using a mechanical lever-arm attached to an axle.

Self-Balancing Nature

Misrepresentation of the loading state due to misalignment of the material sample is taken care of by means of floating cylinder mountings. The cylinders are mounted such that each set from a specific direction are connected to one another by means of compressive bar members. This mounting scheme allows the cylinders to be guided on the same guide rails as the material grips. Misalignment is resolved by the cylinders floating to a neutral position on linear ball bearings.

Linear guidance by means of bearings or bushes is notoriously difficult to execute properly and is prone to stiction issues. To minimise the chance of this occurring, extra precaution was taken to ensure the mitigation of the known causes thereof. The aluminium support blocks that keep the guide rails in place were designed to be custom machined to the required dimensions shown in Appendix C, the correct Bosch-Rexroth hardened steel shafts and linear ball bearings sourced, and the placement and machining of dowel holes emphasised on the drawings and ensured during manufacturing. The machine drawings for parts critical to the functioning of the self-balancing characteristic of the rig are presented in Appendix C. Further, the plane in which the material is loaded acts through the centre of each guide rail, ensuring that no moment acts upon the bearings.

For each of the biaxial directions two similar sub-assemblies are used which

house the linear bearings sliding on the steel guiding shaft and to which the load actuation and material grips are fastened. The CAD model of this assembly is shown in Figure 3.2. The fasteners used to secure the load actuation device as well as the three holes used for securing the material grips are visible in the image.

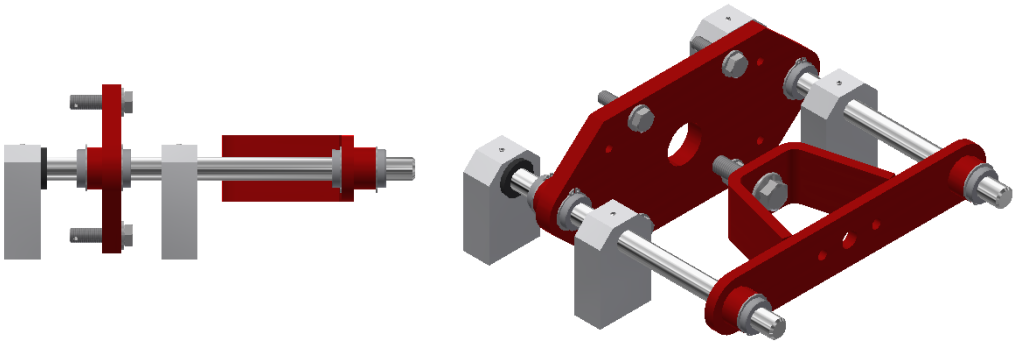

Figure 3.2: CAD model of linear assembly

Shear Loading

One of the biaxial directions has the ability to rotate 30° in total, or 15° to either side of the neutral position, in-plane, around a stationary shaft fixed to the midway point between the two material grips. The neutral position is orthogonal to the stationary biaxial direction. This rotation replicates the method of in-plane shear application used by Cavallaro *et al.* (2007).

Control System

The control system of the BASR is the link between what the user requires and what the rig will execute. A robust system with easy-to-understand interface was implemented.

The BASR has three measurement devices; two pressure transmitters built-in to the pressure regulators used for measuring the pressure within each set of cylinders as well as HBM 4XY strain gauge rosettes for measuring applied torque due to shear loading. No provision is made for the measurement of displacement while the material is loaded. As such, only load-controlled testing can be performed and not displacement-controlled as well. The DIC system

requires that the measured load be synchronised and embedded with the corresponding images. Pressure measurements are ported directly to the data acquisition device of the DIC as a 0-10 V analogue signal. Bridge completion for the strain gauge rosettes is done using a Quantum HBM MX410 dynamic universal amplifier. This device can then output the measured signal as a scaled analogue output of 0-10 V also to be captured using the DIC system's DAQ.

The rig is controlled via a custom made graphical user interface (GUI) which runs the control system in the background and performs the required tasks via a National Instrument USB-6001 device. The programming of the GUI and control system was performed in National Instruments LabVIEW, which is a visual programming language. The Festo MPPES pressure regulators function such that an analogue input of 0-10 V corresponds to a pressure of 0-10 bar. The control system reads the setpoint value for the controller as a Comma Separated Value (CSV) file. This value is output as a voltage of equal magnitude. The pressure regulator responds to this voltage accordingly in order to match the expected outcome. Each regulator has its own control loop with feedback which cannot be adjusted by the user. A second cascaded loop has not been programmed into the user-defined control system. Specific load cases for the various planned tests can be varied by changing the specific file used as the setpoint. The system therefore is load-controlled with an open-loop control system.

3.2.2 Material Grips

Material grips must be able to supply a sufficient clamping load to prevent slipping as well as boundary conditions that can accurately be replicated in an FE analysis. Testing to measure the response of a given material is a process that must be repeated numerous times with different samples. Reducing the time required to load each sample reduces the overall test time. Simplifying the method used to grip the specimen and by ensuring that slight misalignment can be compensated for by another means are some of the methods that can be used to achieve this.

A wrap grip is used in industry when seatbelts require tensile testing. This simple device uses one round roller with a thin slot machined through its diameter. The material is fed through the slot whereafter the roller is rotated

a number of times, wrapping the material around it before being locked into position using pins. Once loaded in the tensile tester the material contracts around the roller, effectively gripping itself. The sharp angle created by the machined slot and the ever increasing circumferential contracting force prevents the sample from slipping if the correct number of rotations is used. The machined slot however jeopardizes the structural integrity of the roller, leading to increased bending which, in turn, changes the strain distribution over the sample. The strain field is seldom of significance in seatbelt testing.

When determining material response using an optical method such as DIC, a strain field disrupted due to the material grips is not desired and will negatively affect the results. In an attempt to reduce this, a design incorporating a second, non-slotted roller, was manufactured. The concept is that the slotted roller, around which the material is wrapped, can slide back and forth in the plane of the applied load. Rotation is prevented by means of machined blocks. The unconstrained translational degree-of-freedom allows the roller to slide against a stationary solid support which can offer added stiffness against bending. This concept is shown in Figure 3.3

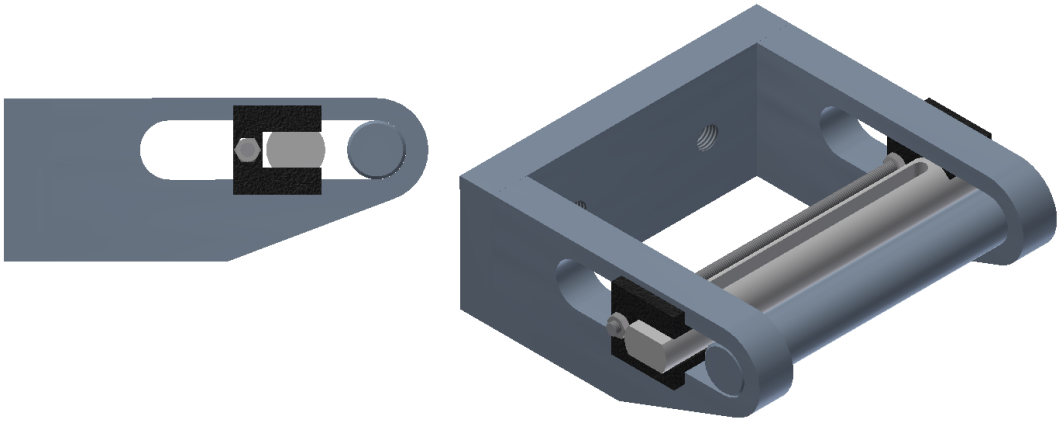

Figure 3.3: CAD representation of material wrap grip used showing both the fixed and sliding rollers as well as the block that lock the sliding roller in place

3.2.3 CAD Representation

CAD models of the floating cylinder sub-assembly and the main frame are shown in Figures 3.4 and 3.5. The complete test rig is shown in Figure 3.6. The

compressive members that connect adjacent floating cylinder sub-assemblies together are indicated as the black bars.

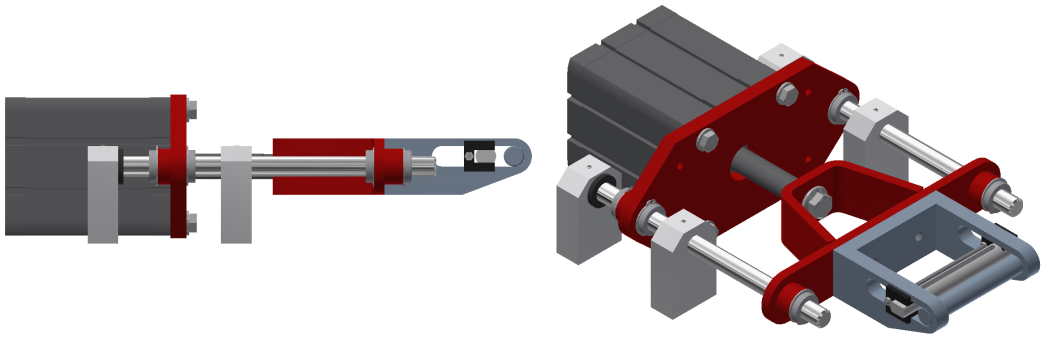

Figure 3.4: CAD representation of sub-assembly consisting of pneumatic cylinder, linear guidance shafts and bearings as well as plate to which material grip is fixed

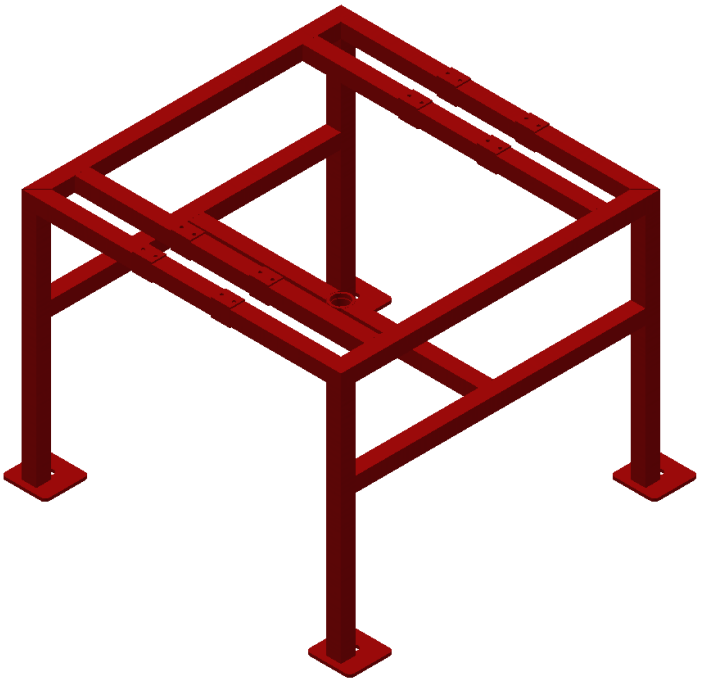

Figure 3.5: CAD representation of the main steel frame to which all separate sub-assemblies are fixed

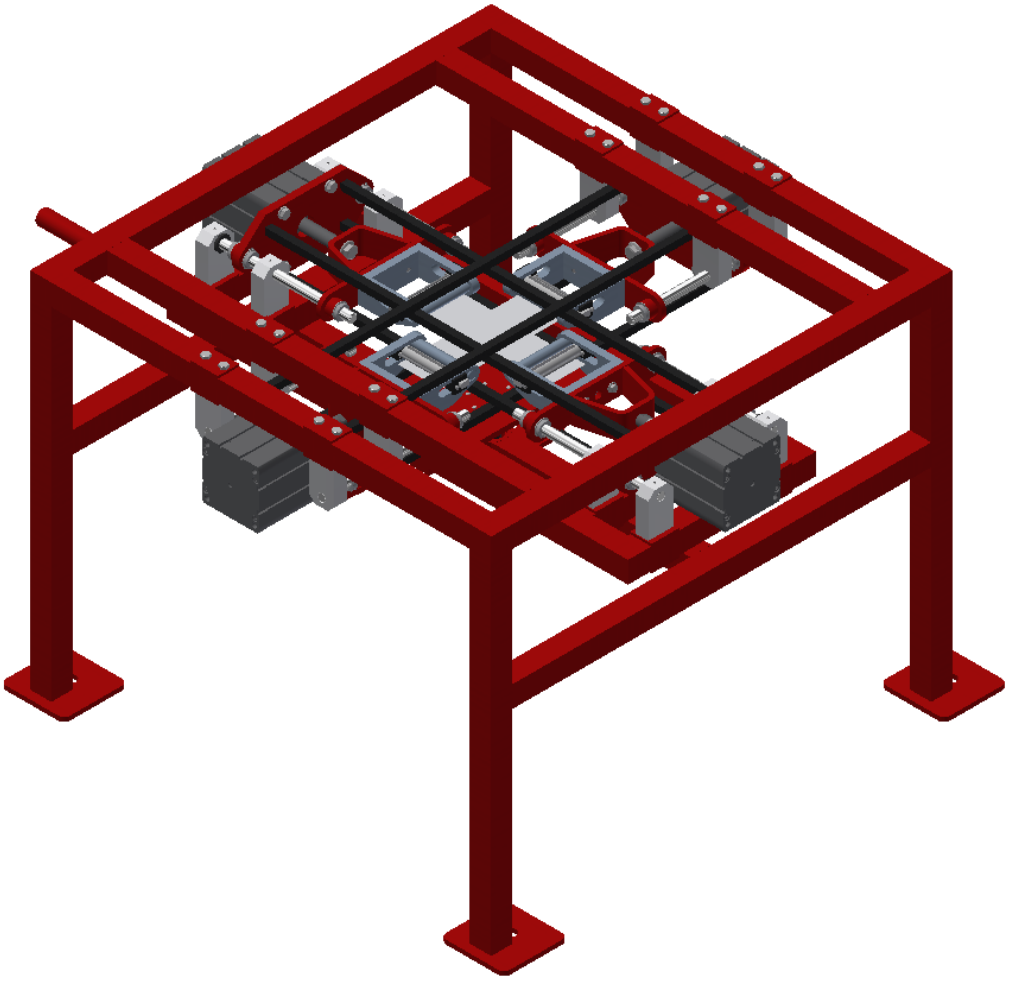

Figure 3.6: CAD model of BASR

3.3 Determining Performance Envelope

Experimental test rigs are designed to be operated within certain physical limitations. These limitations stem from design decisions made prior to manufacturing. Once manufactured, it is required to test the performance limits of the equipment and determine its accuracy. This data set is referred to as the performance envelope of the rig. For this rig the main criteria to test for was the accuracy of the load calculation factor from pressure measurements and performance of the open-loop control system. These factors were tested for individually at first and later as part of a combined test for determining material properties of metallic materials.

3.3.1 Load Calibration

Applied load is calculated using the internal pressure in the cylinders, measured using the built-in pressure sensor of the Festo MPPES regulator, and a linear polynomial. The parameters of this linear fit, along with the sensitivity of this setup to rate of testing, were determined. Fixtures were designed and manufactured to secure a load cell between the cylinders using rod-ends and clevises in order to mitigate the possibility of measuring a moment or tilting load. The test involved a linear ramp from zero to 4000 N using three different inflation rates, ranging from an equivalent 20 N/s to 40 N/s. Each test was repeated four times. A linear fit was performed to relate the voltage measured from the pressure transducer to the force measured by the load cell, as in Eq. 3.1, with Φ_0, Φ_1 representing coefficients, V the measured signal in V, and F the load in N.

$$F = \Phi_0 + \Phi_1 V \tag{3.1}$$

Two different methods of determining these coefficients were investigated: linear least squares regression and robust regression. Least squares regression attempts to minimise the sum of squared differences between all points in the data set and the corresponding linear function. This method relies on the assumption that all entries in the set obey the linear trend with variance that follow a normal distribution. As such, outliers in the data, possibly stemming from measurement hardware errors, violate the underlying assumptions. This violation affects the eventual fit in that each data point carries an equal weight in the sum of squared differences, therefore, outliers that carry a large residual contribute to a large difference and ultimately a skewed model. Short of manually excluding these high leverage data points, the method of least squares offers no way of suitably dealing with them. Robust regression, a form of weighted-and-reweighted least squares regression, however, weighs each data point according to how well behaved it is. As such, it is an iterative process which cannot always be justified computationally. For the application in this thesis the data sets are well suited to robust regression, both for their small size and existence of outliers. The performance of these two methods at calculating the linear fit required is illustrated in Figure 3.7 with the residuals of these fits presented in Table 3.2. Least squares regression delivers a poor fit. Robust regression, however, shows close agreement to the ideal line for all

loads above 300 N. The method of robust regression was therefore used for calculating the coefficients Φ_0, Φ_1, shown in Table 3.1. Both these coefficients were found to be unaffected by load rate and equal for both of the biaxial directions.

Table 3.1: Coefficient values for relating voltage measured by pressure transducer to force in Newton

Coefficient	Value
Φ_0	-161.57
Φ_1	1140.8

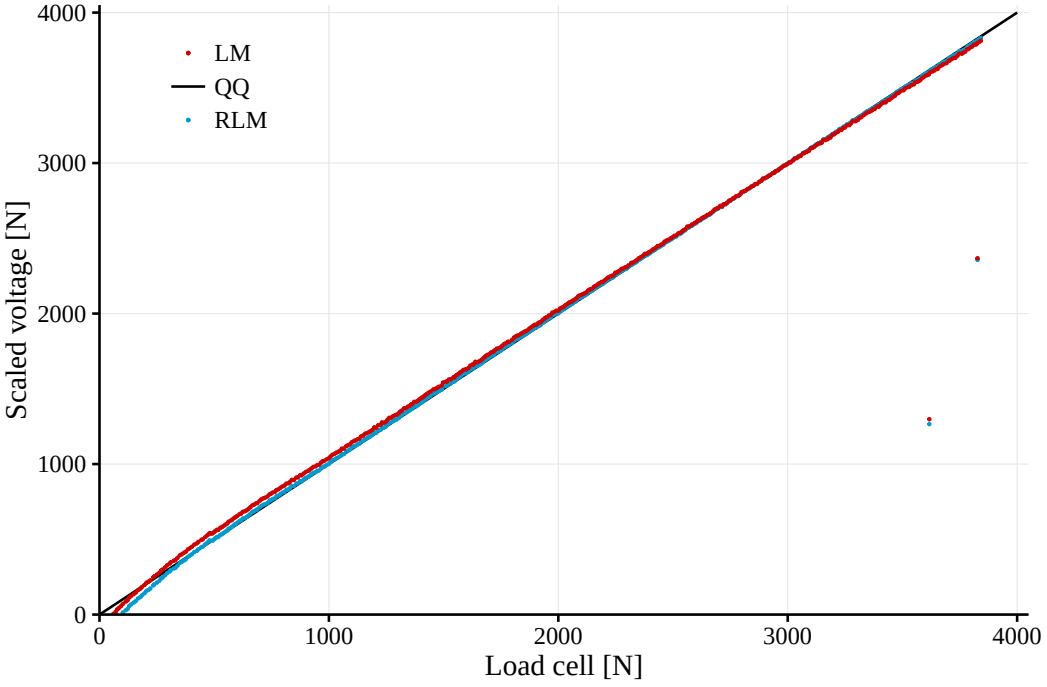

Figure 3.7: QQ plot of linear fit relating measured voltage to force in Newton determined from least squares linear regression (LM) and robust regression (RLM), shown with the ideal fit (QQ)

3.3.2 Setpoint Tracking

An important part of physical testing is being sure that the load case, intended to be applied to a sample, is in actual fact applied correctly. The open-loop

Table 3.2: Residuals from regression fits comparing linear least squares (LM) with robust regression (RLM)

Method	Residual
LM	128.9
RLM	10.41

characteristic of the control system further stresses the importance thereof as any deviation from the intended path cannot be sensed, measured, and corrected while the system is running. To this end, two different load paths were tested. The load path intended for a multi-cycle test, where the load is increased in increments of 20% to a magnitude of 4 V (4400 N), was tested as well as a stepped input with steps equal to 1 V. The measured pressure signal is plotted along with the intended setpoint value in Figure 3.8. Two areas of consistent deviation exist for the multi-cyclic test. The initial inflation from zero pressure lags that of the setpoint value and the initial deflation from maximum cycle load overshoots that of the setpoint. For the stepped input, a much quicker response was required leading to a small overshoot before equilibrium was found. Due to measuring the actual pressure in the system as the test is conducted these deviations will be accommodated for in the final results and further investigation into a method of reducing them not performed.

3.3.3 ASTM E8M Metallic Testing

The efficacy of the rig to determine material properties of a metallic material is used to determine its feasibility for mechanical testing. The ASTM E8M standard and 1000-series aluminium samples are used in conjunction with a conventional displacement-controlled tensile tester, the MTS Criterion Model 44, and DIC to determine the properties of the metallic samples. The MTS and BASR differ fundamentally in their application of the intended load path with the MTS being displacement-controlled and the BASR load-controlled. It is therefore important to attempt to match the strain rates of the two devices, and more importantly, prevent the strain rate of the load-controlled rig from increasing drastically during the near perfect-plastic material response of the 1000-series aluminium.

The test was repeated using the BASR for both of the biaxial directions. Custom grips were manufactured to clamp the aluminium samples in place. In total 30 tests were run shared equally amongst the three devices. The engineering stress-strain curve is shown in Figure 3.9 for each of the devices. Young's modulus and the standard deviation thereof is presented in Table 3.3. Overall very good correlation is evident between the three devices throughout the material response in the elastic and plastic regions.

Table 3.3: Young's modulus and standard deviation thereof as measured using the BASR and MTS

Device	Young's modulus [GPa]	Standard deviation [GPa]
BASR 1	67.87	1.57
BASR 2	66.5	1.32
MTS	68.7	1.02

The near perfect plastic response of the material provides an excellent platform to establish to what extent the strain rate can be controlled in an environment that generally proves difficult for load-controlled test rigs. A series of tests was performed where the strain rate during plastic loading was reduced. Two additional setpoint files were generated where the load rate for the final 25% of applied load was reduced. The load rates for the original test, as well as the reduced rates, are shown in Table 3.4. The results from these tests are shown in Figure 3.10 as strain rate vs strain along with that measured using the MTS. The objective of reducing the strain rate during the plastic regime was met, and in the case of the slowest load rate, reduced below the strain rate measured on the MTS. This shows the capability of the test rig and control system to offer a degree of strain rate control.

Table 3.4: Load rates used during ASTM E8M testing on BASR

Test No.	Load rate [N/s]
I	15.8
II	7.9
III	3.2

3.4 Summary of Test Rig Performance

It was determined that robust regression yielded superior performance in determining the linear fit used to calculate applied load from measured pressure within the pneumatic cylinders. This factor is not dependent on inflation rate within the range tested for. The ability of the pressure regulators to maintain a setpoint value using the control system implemented proved to be satisfactory. Further, the efficacy of the BASR to determine the material response of 1000-series aluminium samples showed close agreement to the results determined following the ASTM E8M standard and the degree of control over the strain rate promising.

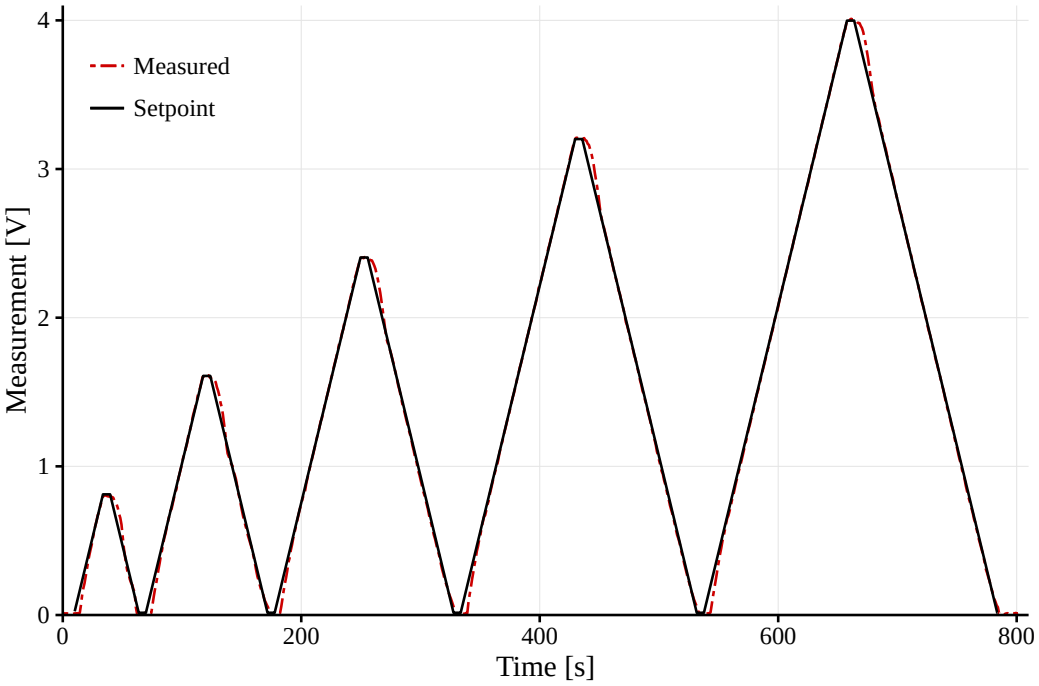

(a) Cyclic load path

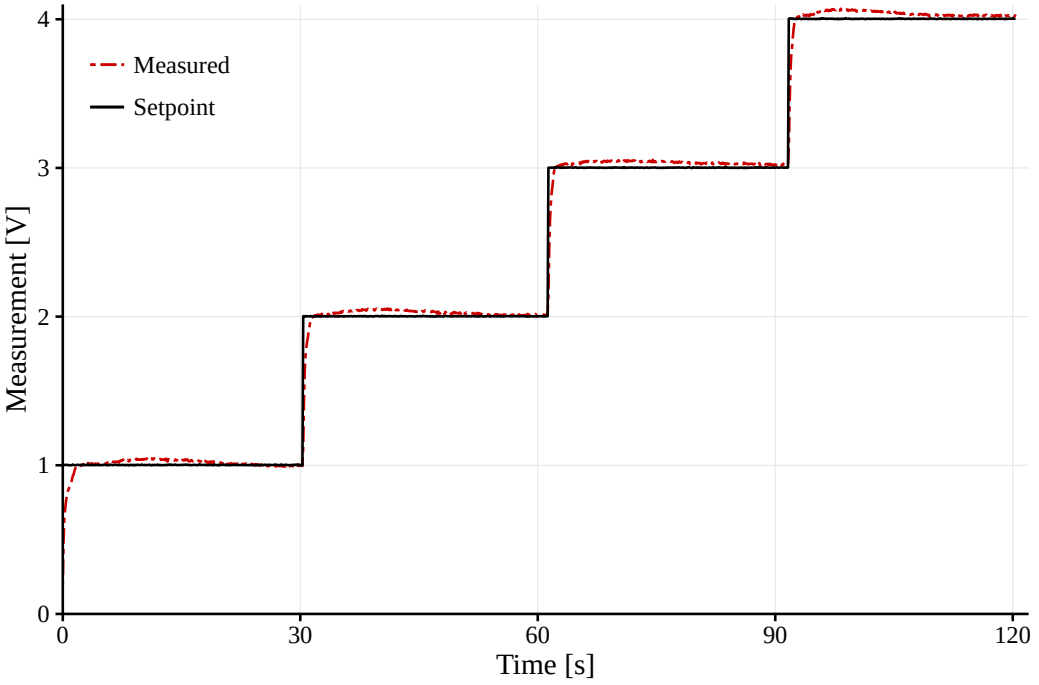

(b) Stepped load path

Figure 3.8: Setpoint value versus actual pressure measurement for various load cases

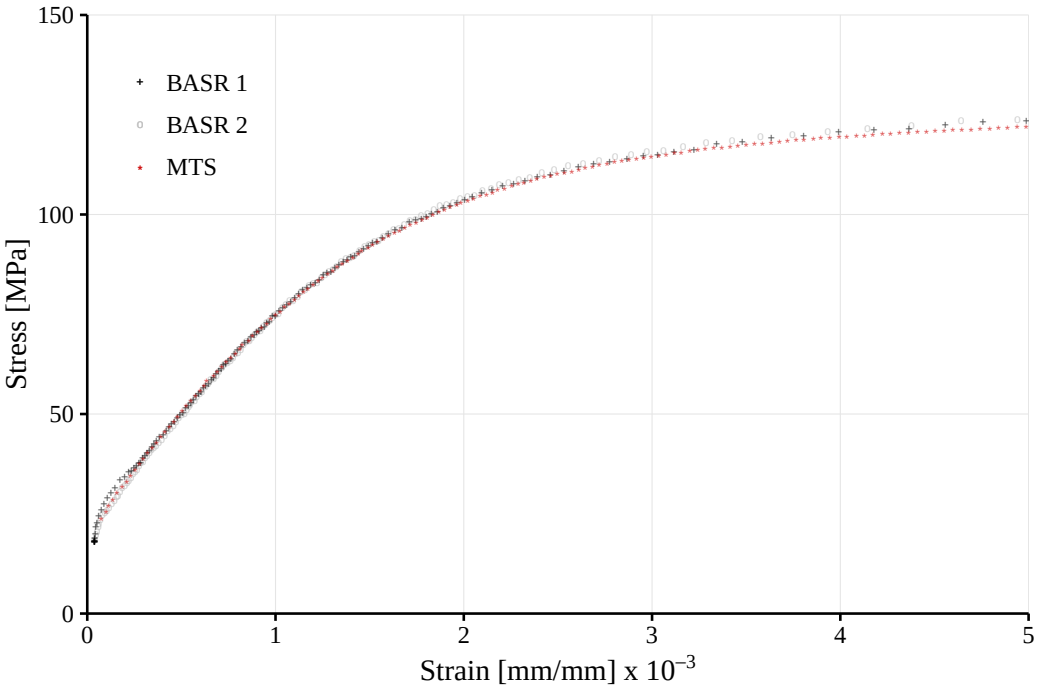

Figure 3.9: Engineering stress-strain curve as tested for using ASTM E8M

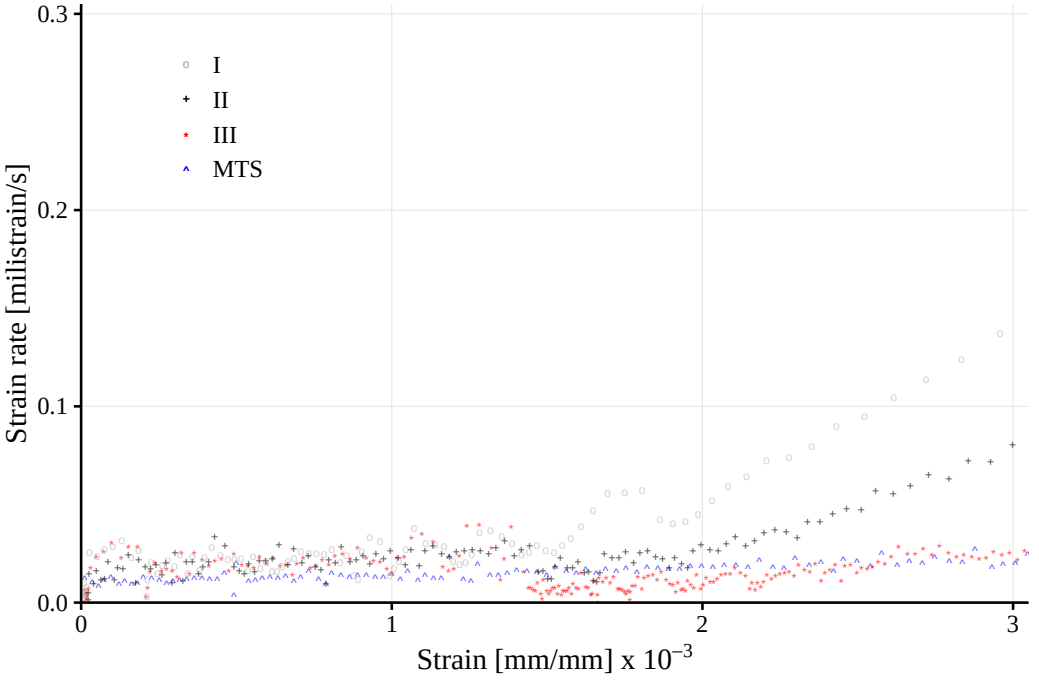

Figure 3.10: Strain rate vs strain of aluminium samples showing the effect of reducing the loading rate, with figure legend corresponding to Table 3.4

Chapter 4

Mechanical Testing of Woven Polypropylene

The biaxial load-unload response of the candidate material is sought for numerical modelling purposes. Currently, no agreed method exists for testing uncoated woven textiles for the required response. Standards available for the tensile testing of textile materials are primarily concerned with the breaking strength and corresponding elongation for uniaxial tests. These standards are available for the testing of textile webbing used for securing cargo and seatbelts (ASTM D6675 - 13 (2013)) or for performing grab tests of fabrics to failure (ASTM D5034 - 9 (2013)). These procedures do not allow for measurement of the load-unload response and are therefore not constructive to this discussion. The details that contribute to the experimental setup and running repeatable tests precede the discussion of exact load cases followed and the results from physical testing.

4.1 Experimental Technique and Preparation

4.1.1 Material Preparation

Meticulous sample preparation is paramount in order to achieve high repeatability between tests (Cao *et al.*, 2008). The immediate mechanical response of polymer materials is highly dependent on environmental factors. Further, the polypropylene of the candidate material is also susceptible to degradation from these factors. Prolonged exposure to ultraviolet radiation, increased humidity

and high temperatures have a detrimental effect on its structural integrity. Virgin material manufactured under constant conditions was sourced from a single supplier in order to alleviate the effects from variance between samples. Further, all tests were performed under similar environmental conditions.

Cruciform samples were cut from a large sheet of the candidate material ensuring that individual tows were continuous along the entire length. The width of the cruciform arms, and therefore the side-lengths of the square area of interest, was kept to within a whole tow of 100 mm. Partially split tows were avoided. Two rows of tows were removed from each of the four edges of the cruciform. When not removed, these edge tows slip out from the weave and lead to an ill-represented geometrical description. The entire sample was then subjected to a manual pre-conditioning load to free fibres from one another in the area of interest. The visco-elasticity of the material demands that the samples lay flat for a sufficient period to relieve the effects of handling and cutting before testing can be conducted. A period of roughly 24 hours was used. A more detailed discussion of sample preparation is presented in Appendix A.

4.1.2 Digital Image Correlation

Digital Image Correlation, the non-contact strain measurement technique used throughout the study, requires a random contrasting pattern, known as a speckle pattern, to measure surface strain on the material. This comparison is achieved by correlating grey-scale intensities of a set of interrogation windows, or subsets, throughout reference and deformed images. This speckle pattern has an effect on the accuracy of the method (Lecompte *et al.*, 2006) and as such, deciding on the ideal speckle for optimum accuracy is currently an area of active research. To this end, a study was conducted to benchmark the technology and the implementation thereof against conventional methods.

Accuracy Benchmarking

A set of tensile tests was performed on aluminium samples using different strain measurement techniques. The devices used were DIC, a clip gauge extensometer, and strain gauges. The same test procedure was followed as for the commissioning of the test rig; the results of which are shown in Figure 4.1.

These results indicate close correlation between the three devices and therefore warrants the further use of DIC for measuring the displacement-field.

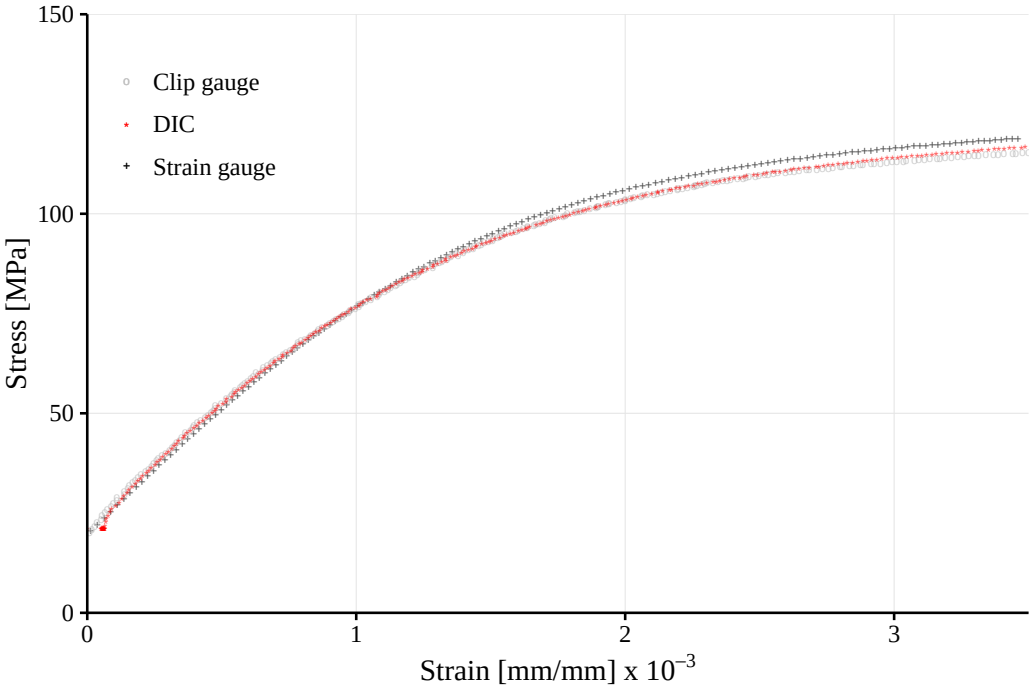

Figure 4.1: Benchmarking of strain measurement techniques including DIC, clip gauge extensometer, and strain gauges

Speckle Quality Assessment

In order to suppress the high reflectivity of the aluminium samples, a matte white base coat was applied before the black speckle was added. The low strains experienced by the sample did not cause paint adherence issues. A frame extracted from the captured images shows the speckle applied on the aluminium in Figure 4.2.

For the polypropylene, three different speckle patterns of various speckle density were tested. Five images of each variation were captured without any load induced deformation. These images were then processed using the DaVis software to calculate deformations. Two different subset sizes were used for each set of images. The deformations calculated by the DIC are erroneous due to no load being applied and therefore serve as a measure of the accuracy of the specific speckle and processing subset. The root mean square (RMS)

Table 4.1: Spurious displacement RMS error for candidate speckle patterns

Relative speckle density	Subset size [Pixel]	RMS δ [μm]
Low	21	0.767
	31	0.533
	51	0.387
Medium	21	0.462
	31	0.333
	51	0.266
High	21	0.436
	31	0.351
	51	0.313

values of the different relative densities and subset sizes are shown in Table 4.1. There is, however, a trade-off; spatial resolution of the data is maximised by reducing the size of the subset, but with this reduction the uncertainty in the strain calculation increases due to a reduced number of unique features within each subset (Crammond *et al.*, 2013). The results indicate that the medium relative density yielded the lowest RMS value. However, this pattern was difficult to apply in a repeatable fashion.

The speckle pattern shown in Figure 4.3 has the highest relative speckle density of those tested for and has a high repeatability in its application. The RMS value of the error is slightly higher than for the medium density case, but the difference is negligible. Further, the small loss in accuracy between subset sizes 31 and 51 is accepted for a return in increased spatial resolution. This pattern is applied as a lightly misted coating where the paint is allowed to effectively stain the material as opposed to a thick layer of paint. The individual speckles applied directly to the surface of the polypropylene attempts to mitigate the adherence issues.

Application of Technology

The lighting conditions were kept constant throughout testing. Testing was performed during night hours to avoid the changing position of the sun hindering lighting. Fluorescent tube lights flooded the laboratory to prevent the necessity of using additional LED flash lights. The LED flash lights were prone to causing reflections on the material surface ultimately jeopardizing the calculation of the displacement field from the captured images.

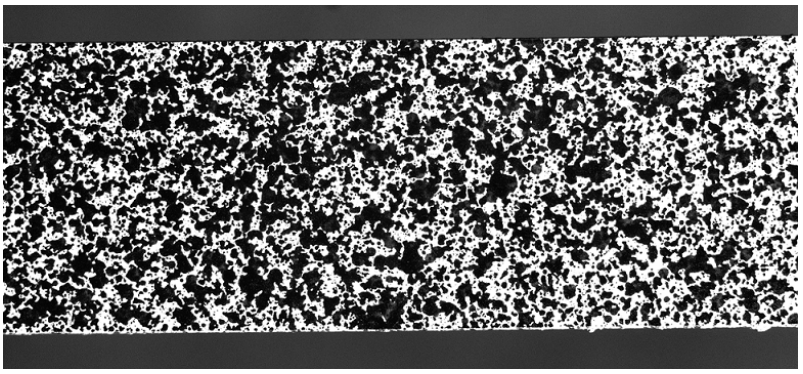

Figure 4.2: Contrasting speckle pattern applied to aluminium sample, shown in the horizontal position, with cross-sectional width equal to 12.5 mm

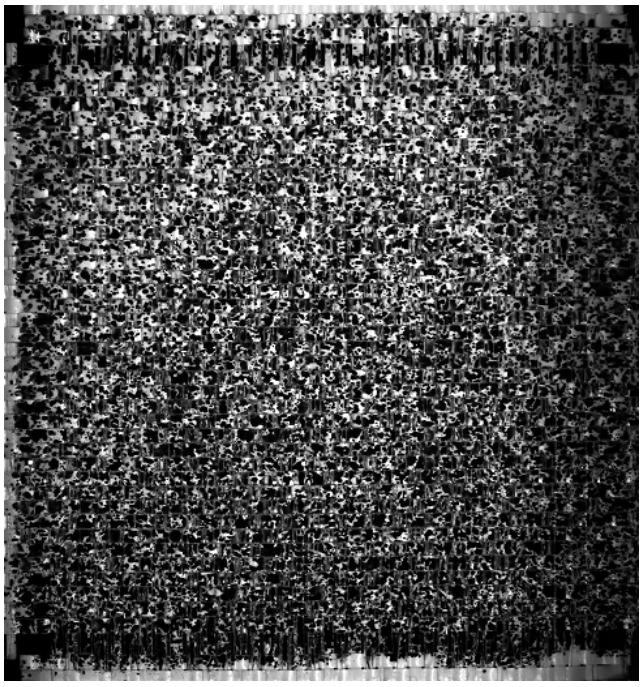

Figure 4.3: Contrasting speckle pattern applied to polypropylene sample measuring 100 mm square

The close correlation amongst the devices tested indicate that the contrasting random speckle pattern applied is sufficient for strain measurements and that the DIC technology as a whole can be utilised for surface strain measurements in this project.

4.1.3 Determining Cross-Sectional Area

The woven nature of the material does not lend itself to simple through-thickness measurements required for the calculation of the cross-sectional area on a prepared sample. Instead, individual tows are removed and measured separately for thickness and width. The results of multiple measurements along a 300 mm section of tow for multiple tows extracted from the specific material direction are averaged to determine both the tow thickness and width. Tows in the MD remain flat and smooth during weaving leading to highly repeatable measurements. CD tows, however, are crunched up to a large extent during the manufacturing process. Thickness measurements from these tows, as removed from the fabric, lead to scattered and unrepresentative measurements. Instead, these tows are flattened to mimic their counterparts before being measured. This step requires that the width of the flat tow be recorded as well. The theoretical width of a cruciform sample, if calculated using the measurements of a flattened tow as well as the number of tows, exceeds that of the physical sample. It is therefore assumed that the integrity of those crunched tows remains intact after weaving and can be represented using a flattened tow. A micrometer was used for thickness measurements and a vernier calliper for the width measurements. The number of tows that constitute a prepared cruciform prior to testing was recorded for each material direction.

Equations 4.1 and 4.2 are used for calculating the cross-sectional area of the respective material directions. Table 4.2 shows the averaged results for individual tow measurements as well as the averaged cross-sectional area for the two material directions.

$$A_{MD} = 2t_{MD}N_{MD}w_{MD} \tag{4.1}$$

$$A_{CD} = t_{CD}N_{CD}w_{CD} \tag{4.2}$$

Where A is the cross-sectional area, t the tow thickness, N the number of individual tows, and w the flat tow width. The extra scale factor that is multiplied in Eq. 4.1 represents the doubled-up tow architecture utilised in the material MD.

Table 4.2: Measurement of individual tow geometries for calculation of averaged cross-sectional area in material MD and CD

Direction	Thickness, t, [mm]	Width, w, [mm]	No. tows, N	Area, [mm^2]
Warp	0.12	2.4	38	21.89
Weft	0.086	4	37	12.73

4.2 Scope

The focus of physical testing is on determining a method that will better improve the numerical implementation thereof. Extensive testing to gain an exact understanding of the material response under various loading conditions is beyond the scope of this research. These excluded factors include creep measurements, shear response and extensive load ratio testing.

4.3 Design of Test Procedure

The test procedure was designed using information from both literature and preliminary testing. The effects of various loading conditions and load paths were investigated. A comparison between the measured results from using a single-cycle load path to those from a multi-cyclic load path was required. The experimental setup used and a step-wise description of the testing process are available in Appendix A.

4.3.1 Cyclic Load Paths

In general, uncoated woven textile testing is conducted in a manner that attempts to assist the characterisation thereof as part of a numerical simulation. Two fundamentally different load paths are often utilised; single- and multi-cyclic loading. The single-cycle path loads the cruciform sample to a maximum

load below that of the ultimate tensile load of the material whereafter the load is gradually removed back to zero. Multi-cyclic loading is implemented in literature using a vast array of variations, but essentially attempts to capture the load-unload path at a number of intermediate loads to that of full-load.

Single-cycle loading to capture the material shear response was attempted by Cavallaro *et al.* (2007). They were not concerned about the biaxial tensile response of the material, but instead investigated the effect different pretensions had on the shear behaviour. Multi-cyclic loading was undertaken by Chen *et al.* (2015). They used a load profile where a pretension is enforced on the sample whereafter the load is increased above and decreased below that of the pretension, in cycles. Each of the two methods has its drawbacks. Single-cycle loading is very time efficient, but is not accommodating in capturing the unload path for loads intermediate to that of the full-load. Multi-cyclic loading often times leads to a measured material response that is difficult to process and characterise in order to utilise in a material model. Further, depending on the test specifics, running multi-cycle tests can be time consuming. The application of both these methods was tried during this research and the measured results were investigated.

4.3.2 Preliminary Testing

Preliminary testing helped identify certain characteristics of the material and isolate material response as artefact of the test rig and procedure. This process aided the design of the final procedure required for the numerical implementation thereof. Results from this phase of testing are from cruciforms prepared from a previous variant of the candidate material.

Initial Response

An initial single-cycle test was run to gather results from which further characteristic testing could be designed. For this test, the applied load gradually increased to a maximum value over 150 s, held for 40 s at that load, and gradually released to zero over 150 s. The load-strain curve for both material directions is shown in Figure 4.4. Results show a near linear material response during loading from 1000 N onwards, a nonlinear response during unloading, with noticeable permanent deformation at zero-load as well as intriguing be-

haviour where the load direction is switched. The initial nonlinear response during loading at low stresses and the subsequent linear behaviour above an apparent threshold was found by Hu (2004) to be a characteristic of woven materials. The behaviour near the switching point exists as two parts; the first is the horizontal section, a scenario where the material strains under a constant load and the second being the near vertical drop where a reduction in load does not correspond to a noticeable reduction in measured strain. These two occurrences were tested further to identify a time-related connection.

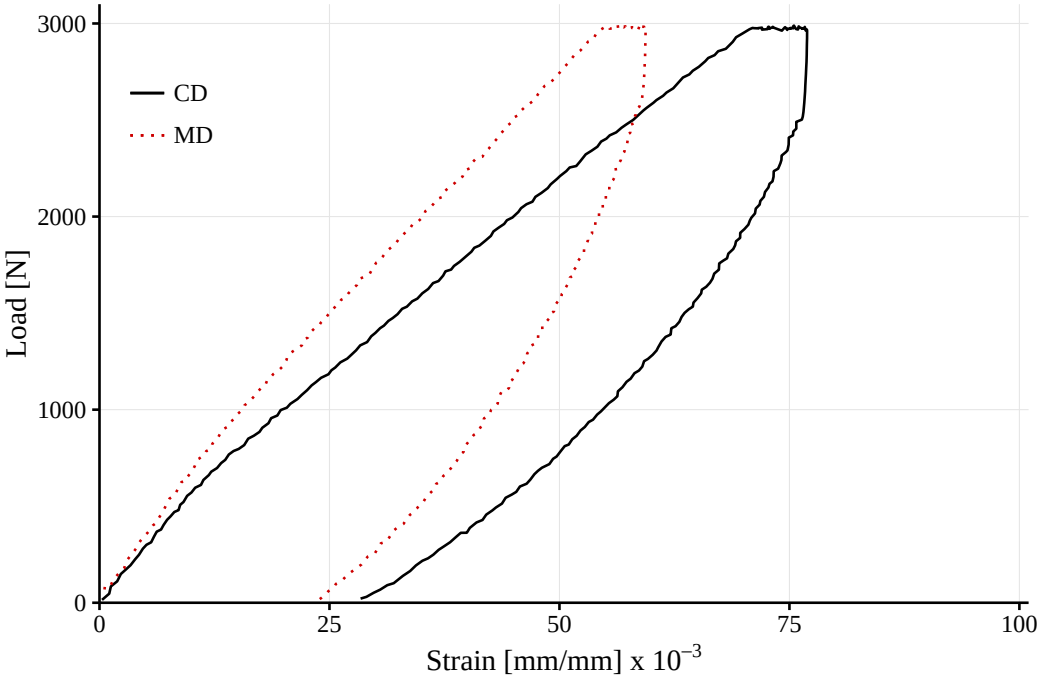

Figure 4.4: Single-cycle load-strain curve for initial test

Time-Dependent Response

The behaviour of the load direction switching point was investigated using a multitude of load cases designed to highlight a time-dependent response of the material. Essentially, the effect of creep is investigated by varying the time that the maximum load is applied as well as the time to unload from that maximum value. A summary of the differences between the load cases is shown in Table 4.3.

Table 4.3: Summary of load case design variations

Test case No.	Time [s]		
	Load	Hold	Unload
Initial baseline	150	40	150
I	150	0	150
II	150	600	150
III	150	360	360
IV	150	0	720

The results of the load cases summarised in Table 4.3 are shown in Figure 4.5 for the material cross-direction (CD). The material response during loading to the maximum value is consistent for all samples. A pronounced amount of creep is evident for the load cases where the maximum load was sustained for an extended period of time. The initial reduction of load is dominated by the phenomenon where no apparent reduction in strain follows; instead, a vertical drop is evident on the load-strain curve. This phenomenon is not necessarily related to the rate at which load is reduced, evident by the slight difference between load cases I and IV, and the non-existent difference between load cases II and III. The difference in unload paths between load cases I and IV can be attributed to creep at sustained higher loads, even during material unloading. Hu (2004) found this vertical drop to be a characteristic of textiles.

Single- versus Multi-Cyclic Response

The dependence of the material response to the cyclic nature of loading was investigated. The numerical modelling approach, presented in the succeeding chapter, requires only the response measured during a single-cycle load. It is therefore necessary to demonstrate the impact of the load path on the final response.

A set of tests was run under similar environmental conditions using both the load paths. The single cycle test follows the load path used for the initial baseline test in the preceding section. The multi-cyclic test ramps the applied load to the maximum required load in incremental step sizes of 20%. After each increment the load is reduced to zero before the next cycle commences. A comparison of these approaches is shown in Figure 4.6. These results indicate

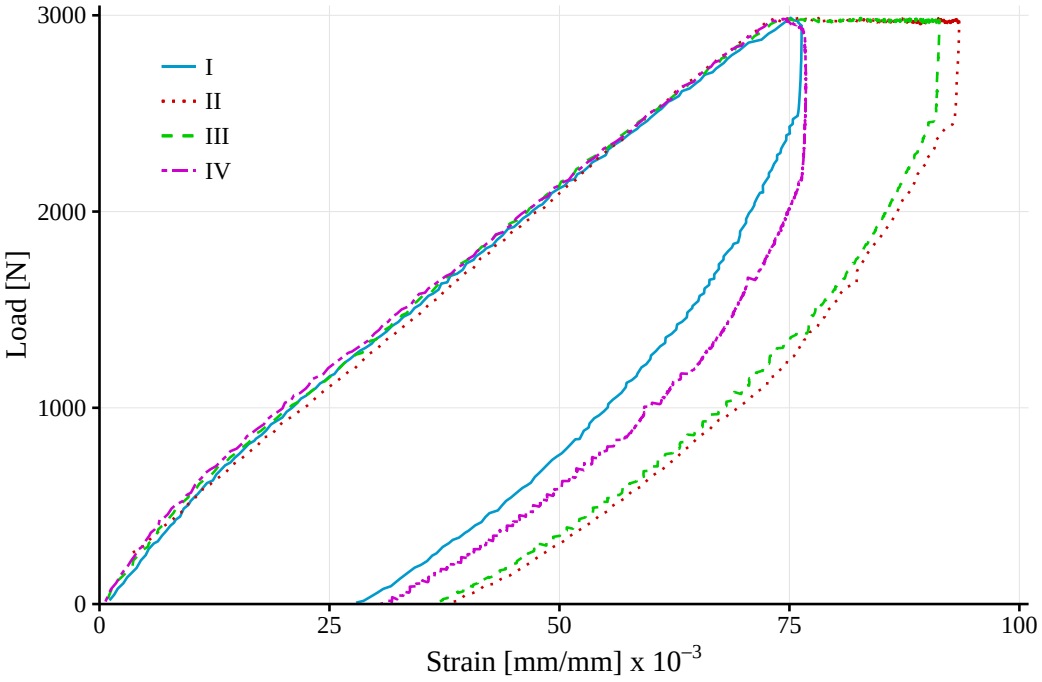

Figure 4.5: Single-cycle load-strain curve showing time-dependent response for material CD

that the response of the multi-cyclic load path fits within the envelope from that measured during a single-cycle test. The permanent deformation once loading has been removed is identical for both the load paths in the respective material directions. During multi-cyclic testing the material stiffness increases with every cycle, as evident by the increasing slope of the load path. However, the maximum strain measured for that cycle matches that for the single-cycle test at a similar load. Material response is ultimately not largely altered by the cyclic nature of the load path.

4.3.3 Finalised Testing Load Profile

The data gained during preliminary testing aided in designing a load profile that would allow the extraction of the sought after material response within the project scope. A single-cycle load path is implemented. The effect of time-dependent material response is kept to a minimum by reducing the 40 s pause at maximum load to 3 s. This short pause ensures the pressure within the system reaches the required magnitude during each test, but prevents material creep from interfering with results to a noticeable extent.

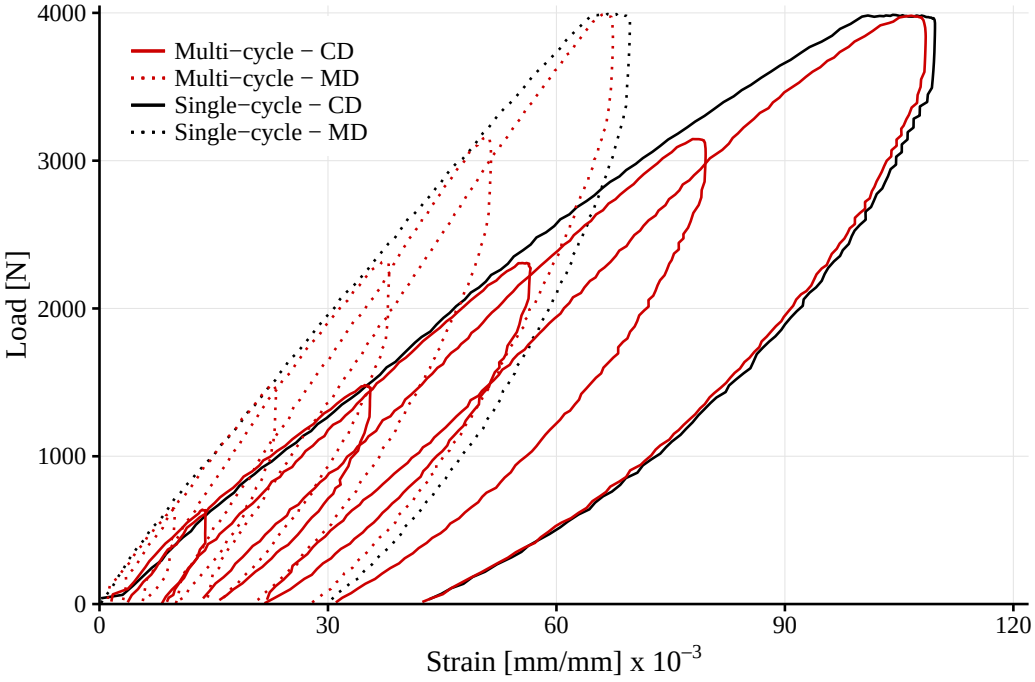

Figure 4.6: Comparison between single- and multi-cyclic load paths

An illustration of the normalised load case plot against time is shown in Figure 4.7. The load path for loading and unloading is shown as well as the overall test duration. The maximum load can be adjusted via the GUI of the test rig. This adjustment is a factor applied equally to all entries in the file used as set point and does not alter the duration of the test. The duration of the test is such that the strain rate should not lead to measuring rate-dependent material properties stemming from the visco-elasticity of the candidate material.

The orientation of the two material directions in the application of inflatable dunnage bags is usually such that the CD withstands the hoop stresses and the MD the longitudinal stresses. This non-ideal loading scenario, where the weaker material direction is used to withstand the higher stress, stems from limitations in the manufacturing process that weaves the bag as a continuous cylinder. Load ratio testing is therefore conducted in a fashion where the CD is always subjected to the highest load amongst the two material directions.

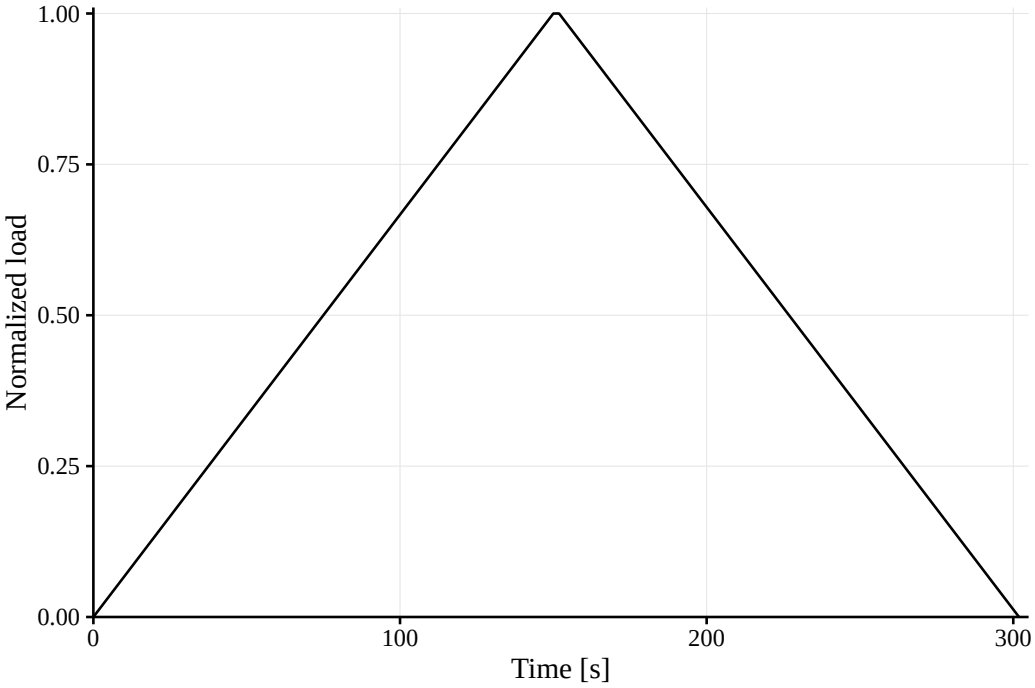

Figure 4.7: Normalised final load case for single cycle testing showing test duration and load path

4.4 Results

All physical testing was performed to minimise discrepancies stemming from variations in the testing procedure; the previously presented load case applied to cruciform samples prepared from identical material tested during similar environmental conditions are presented and discussed. Results in this section are from cruciforms prepared from high quality, specially sourced material.

4.4.1 Intermediate Single-Cycle Testing

Material response to loads intermediate to those where the load cycle is continued to the region near expected failure, was tested for. These results are used as leverage in the succeeding chapter in aiding the presented numerical response modelling approach. To this end, multiple separate cruciforms were tested for load-unload response at intermediate loads. Samples were removed after being subjected to a single intermediate cycle. In total three loads intermediate to the full load were tested, shown for both material directions as averaged results of four repeated tests in Figure 4.8. Results show repeatable

behaviour during the loading phase of all samples for both material directions. Further, the unload profile of each load increment is roughly similar in shape.

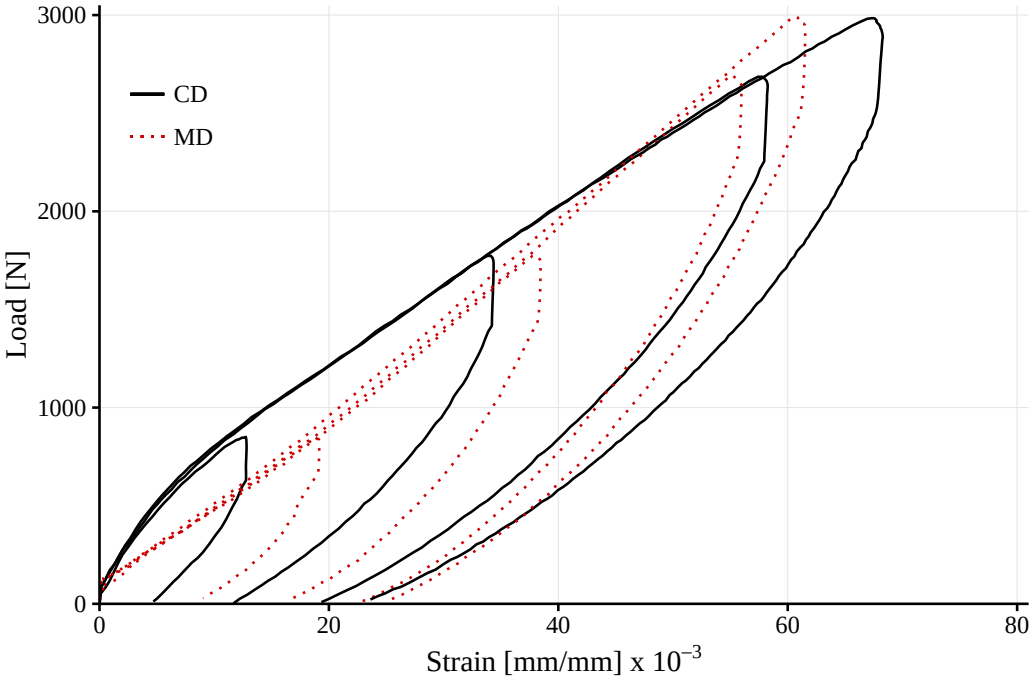

Figure 4.8: Load vs strain results from single-cycle testing cruciform samples at loads intermediate to the full-load cycle

4.4.2 Full-Load Single-Cycle Loading

Investigating the behaviour of the coupled material response between the CD and MD requires that the biaxial load ratio be varied amongst different tests. The load ratio, summarised in Table 4.4, was varied to represent the material orientation in the physical inflatable structures where the weaker CD is subjected to a higher load. Figure 4.9 shows the load vs strain results for the CD and MD, respectively.

Table 4.4: Different biaxial load ratios tested

Load ratio No.	Biaxial load ratio [CD:MD]
I	3000:3000
II	3000:2500
III	3000:2000
IV	3000:1500

The extent of coupling between material directions is not as pronounced as has been noted in literature. This coupling is predominantly driven by crimp interchange, and as such, varies amongst different weaving machines and material architectures as each material is tailored for its intended application. Nonetheless, a clear trend is evident in the maximum measured strain in Figure 4.9a and the maximum applied load in Figure 4.9b. A decrease in load applied to the MD leads to a higher measured maximum strain in the CD. Further, for the load cases where the load ratio is large, the material initially contracts such that a negative strain is measured. This phenomenon indicates the crimp content of the CD being inherited by the MD before the load applied in that direction is great enough to overcome the interchange.

The load-controlled characteristic of the test rig has the possibility of a situation resulting where a material is tested at a rapidly increasing strain rate. Figure 4.10 shows the strain and strain rate plot versus time, respectively. The gradual increase in strain evident in Figure 4.10a indicates a situation where a stable strain rate results. Figure 4.10b shows stable strain rate as an increase to a constant value for the duration of the loading part, where after a gradual increase in the rate, measured as a negative quantity, for the unload section is shown. This trend is evident for both material directions and indicates that strain rate never reaches a runaway state, but rather proceeds in a controllable fashion. Material properties related to visco-elasticity are therefore not measured unbeknownst.

4.4.3 Deformed Displacement Distribution of Samples

Ensuring that samples are loaded in the desired manner is crucial when selecting the area for which strain is calculated. Highly non-uniform deformations can lead to erroneous strains when included within that area. The displacement-field of the deformed samples at maximum applied load is shown in Figure 4.11 for both material directions, respectively. Both fields show high uniformity, especially within the central region. A constant change from the maximum to minimum deformation is evident. Figure 4.12 shows the fields combined for both of the material directions.

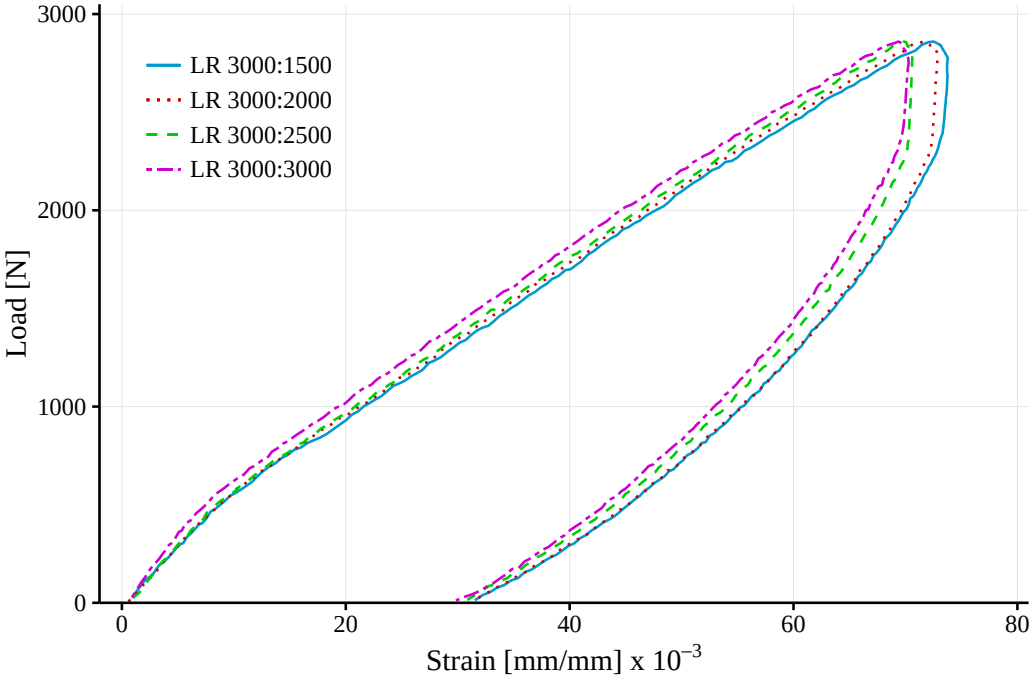

(a) CD

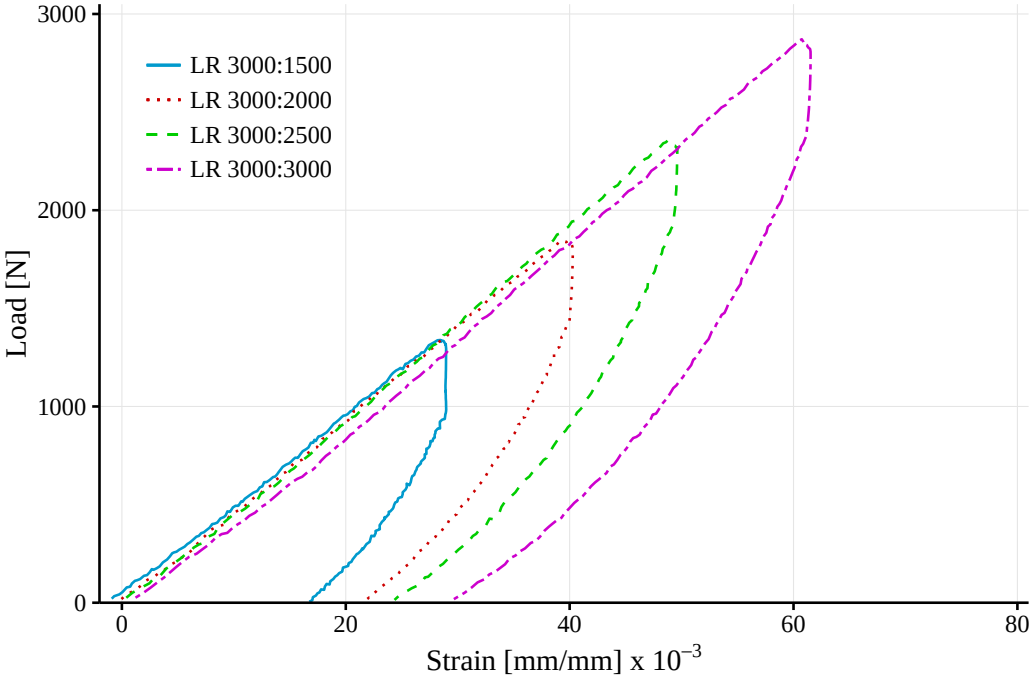

(b) MD

Figure 4.9: Combined load vs strain results of various biaxial load ratio testing shown independently for the material directions, with figure legend indicating the maximum applied loads as CD:MD

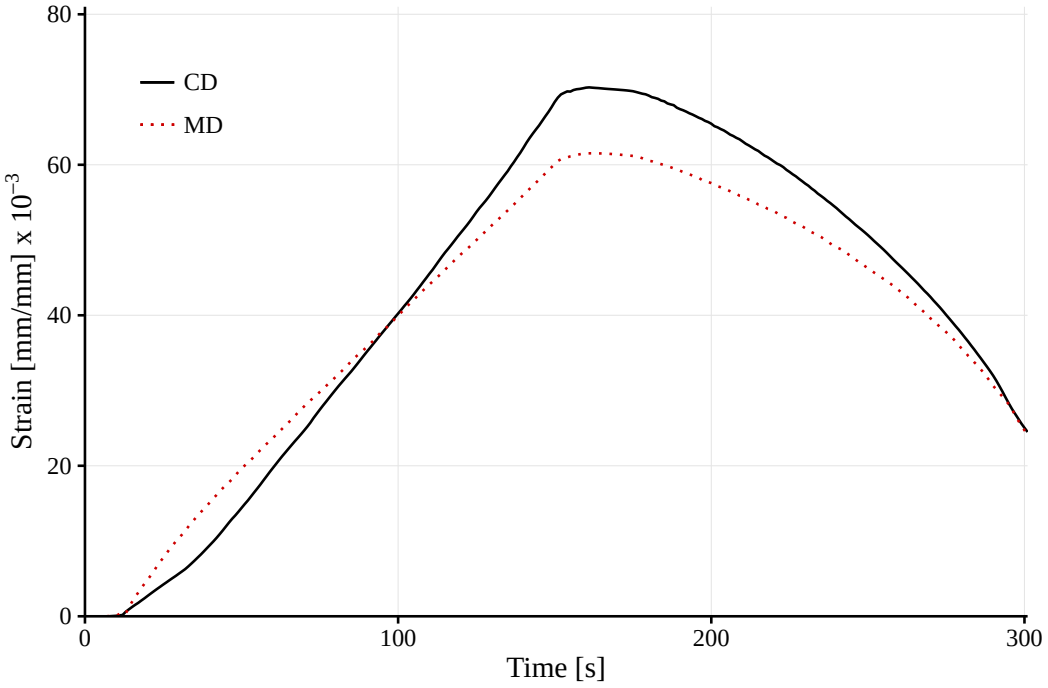

(a) Strain vs time for both material directions at 1:1 load ratio

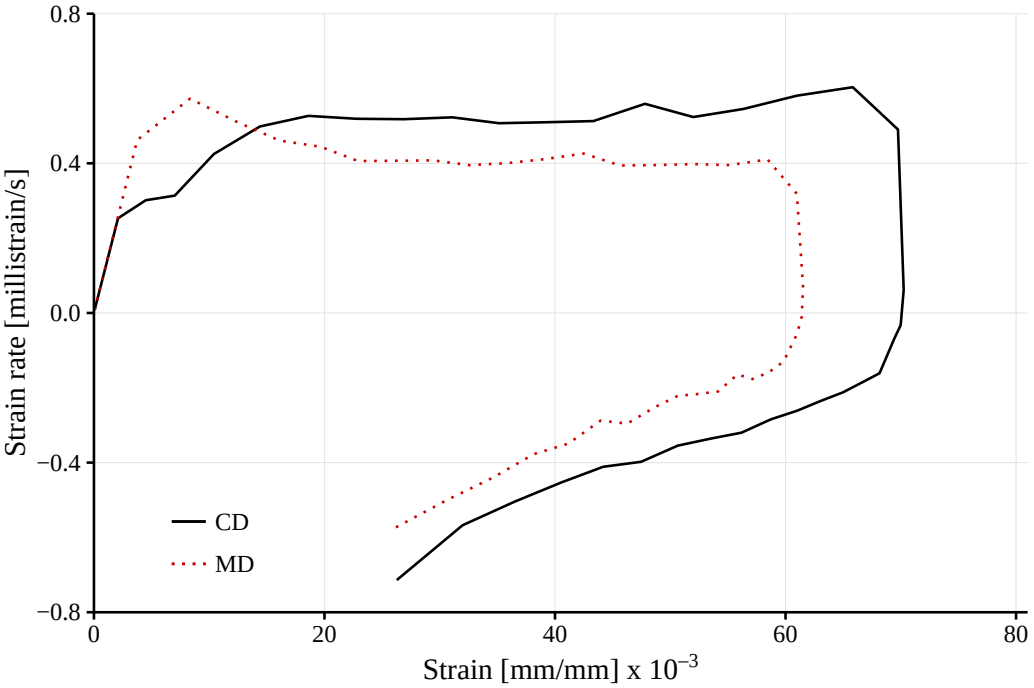

(b) Strain rate vs strain for both material directions at 1:1 load ratio

Figure 4.10: Time related material response

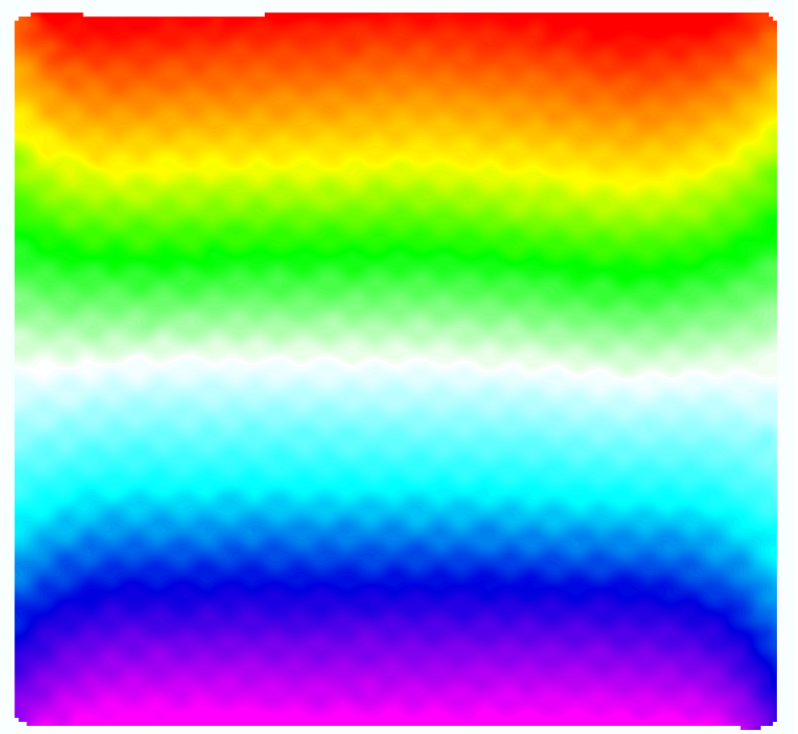

(a) CD

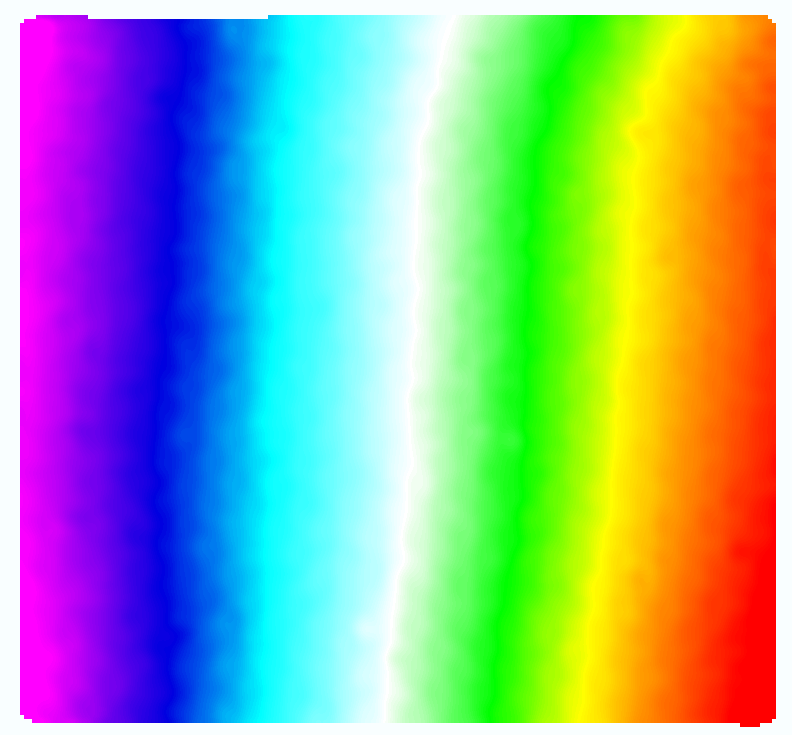

(b) MD

Figure 4.11: Displacement-fields separated for both material directions, shown as a plot of the maximum (red) and minimum (purple) displacements

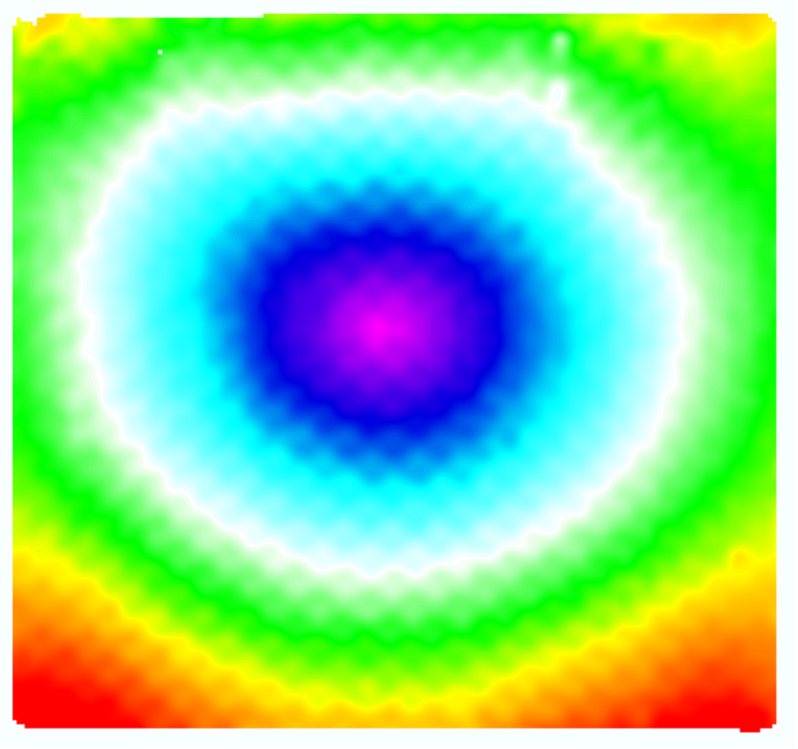

Figure 4.12: Displacement-fields combined for both material directions, shown as a plot of the maximum (red) and minimum (purple) displacements

4.4.4 Results Repeatability

The meso-scale architecture of woven polymers and the variation of material properties along the length of individual tows lead to inconsistent response measurements at the fabric level. During this study results for every unique load case are presented as the averaged results measured during four individual tests using different cruciforms. Accounting for the variance between subsequent tests stemming from variability in the material is not within the scope of this project. The variance between tests is shown in Figure 4.13 for both the material directions as measured during the load ratio testing case of 3000:2500. The trend evident while comparing results from different load ratios holds true for these results; a lower strain in the MD results in a higher strain for the CD. The difference between the maximum strain for the highest and lowest measured tests is 5% for the CD and 6% for the MD.

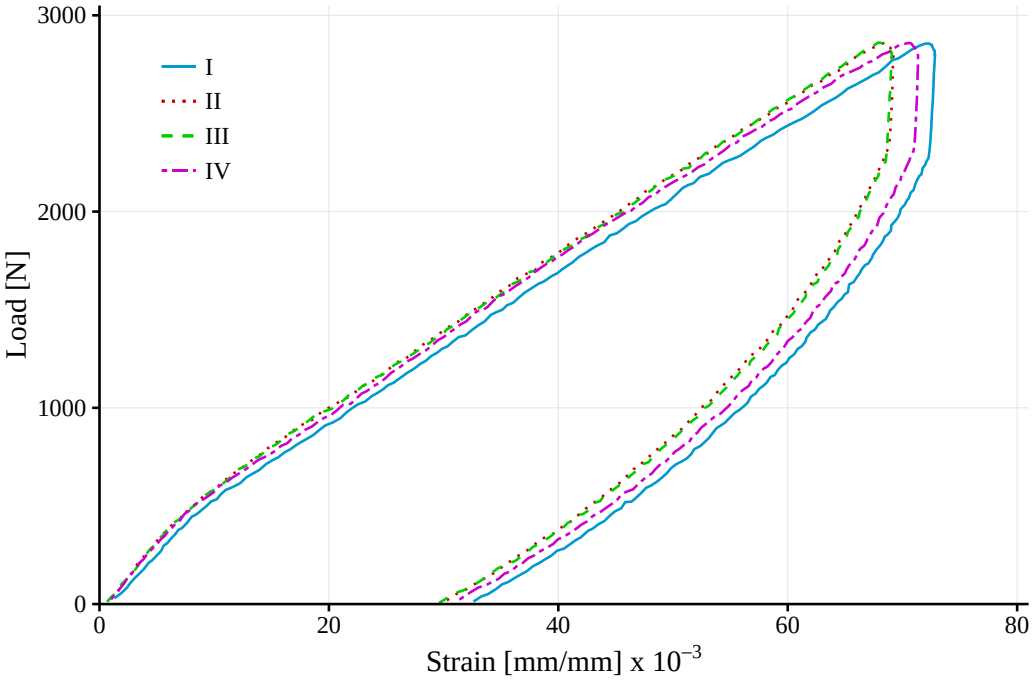

(a) CD

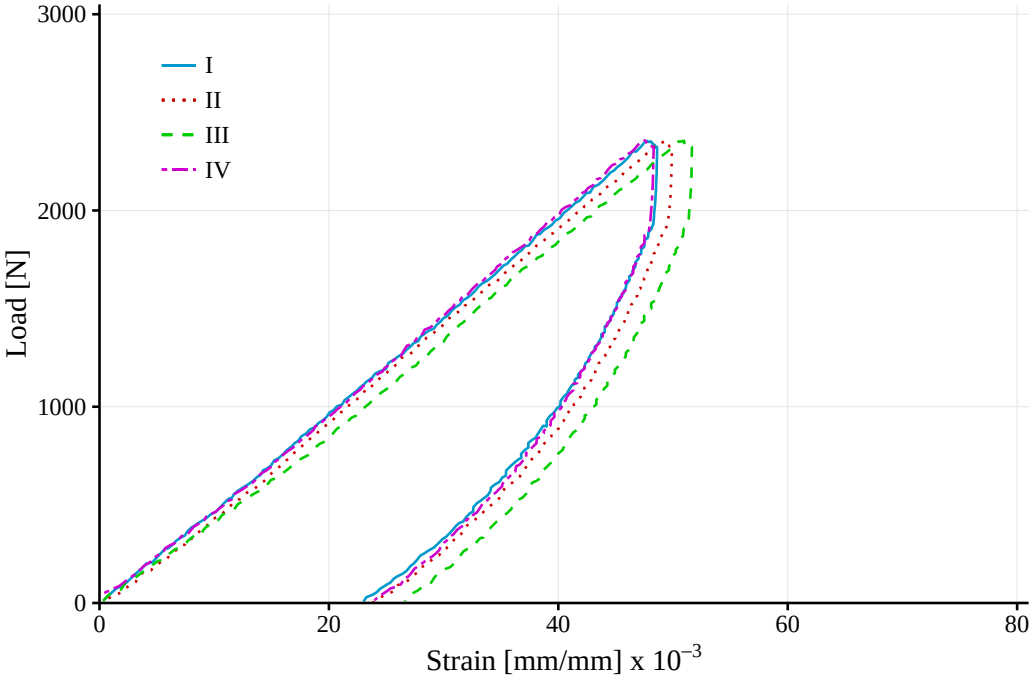

(b) MD

Figure 4.13: Physical test repeatability of candidate material in both material directions shown for four tests

Chapter 5

Response Modelling and Initial Numerical Implementation

Woven polypropylene does not lend itself to being modelled within the FE environment using standard material models available. Models created specifically for woven textiles incorporate too high a level of detail to be considered for large structures. Further, the variation in material characteristics for woven polypropylene intended for similar applications is sufficiently large that it cannot warrant modelling the intricacies of the textile kinematics. A method that models the material behaviour for numerical implementation is presented where a results-orientated strategy is followed. This involves modelling the results of the material response to mechanical loading and using that as the constitutive law relating stresses to strains. A unique method, where a material model is generated from results of a single-cycle test, is presented where intermediate loads can be accounted for during the unload path.

5.1 Overview of FE Implementation Requirements

In structural analysis, a model that demonstrates nonlinear behaviour drastically increases the effort to set-up and the computational requirements to solve. A linear analysis requires only one computation for the solution. In nonlinear analyses, the stiffness matrix is a function of the applied loads and deformations. They are solved by dividing them into a series of increments which are

solved as if linear. At the end of each increment the geometry is updated and used to recalculate the structure stiffness matrix. For implicit FE solvers, an iterative solution subject to a convergence criterion is required to solve each increment, such as the Newton-Raphson approach. Nonlinearity in the models arise from material, geometric or boundary conditions. The material response presented in the preceding chapter, along with the large geometric changes that structures utilising woven textiles as reinforcement undergo, warrants the use of nonlinear FE analyses.

A brief overview of the FE method is given, adapted from Cook *et al.* (2002), in order to clarify at which stage of the solution, and how the material response is incorporated. The governing equation of a linear static FE analysis is shown in Eq. 5.1, where $\mathbf{K}$ is the structure stiffness matrix, $\mathbf{d}$ the nodal displacement degree-of-freedom vector, and $\mathbf{r}$ the external force vector applied to the structure nodes.

$$\mathbf{Kd} = \mathbf{r} \tag{5.1}$$

The structure stiffness matrix, $\mathbf{K}$, is assembled from the elemental stiffness matrices, $\mathbf{K_e}$. Membrane elements are considered for this study, therefore, for a bilinear rectangle four node displacement-based plane element with eight d.o.f., shown in Figure 5.1, the element stiffness matrix is given by Eq. 5.2. $\mathbf{B}$ is the spatial derivatives of the field variables matrix, $\mathbf{E}$ the matrix of elastic stiffnesses, and t the element thickness. Element strains in terms of nodal d.o.f. are related by means of $\mathbf{B}$ according to Eq. 5.3.

$$\underset{8\times8}{[\mathbf{K_e}]} = \int_{-b}^{b}\int_{-a}^{a} \underset{8\times3}{[\mathbf{B}]^T}\ \underset{3\times3}{[\mathbf{E}]}\ \underset{3\times8}{[\mathbf{B}]}\ t\ dx\ dy \tag{5.2}$$

$$\boldsymbol{\varepsilon} = \mathbf{Bd} \tag{5.3}$$

The elastic stiffness matrix for an orthotropic material under plane stress conditions, shown as a constitutive equation relating stresses to strains, is given in Eq. 5.4 and 5.5

$$\begin{Bmatrix} \varepsilon_x \\ \varepsilon_y \\ \gamma_{xy} \end{Bmatrix} = [\mathbf{E}]^{-1} \begin{Bmatrix} \sigma_x \\ \sigma_y \\ \tau_{xy} \end{Bmatrix} \tag{5.4}$$

$$\mathbf{E}^{-1} = \begin{bmatrix} 1/E_x & -\nu_{yx}/E_y & 0 \\ -\nu_{xy}/E_x & 1/E_y & 0 \\ 0 & 0 & 1/G \end{bmatrix} \tag{5.5}$$

with E the stiffness modulus, ν the Poisson's ratio and G the shear modulus.

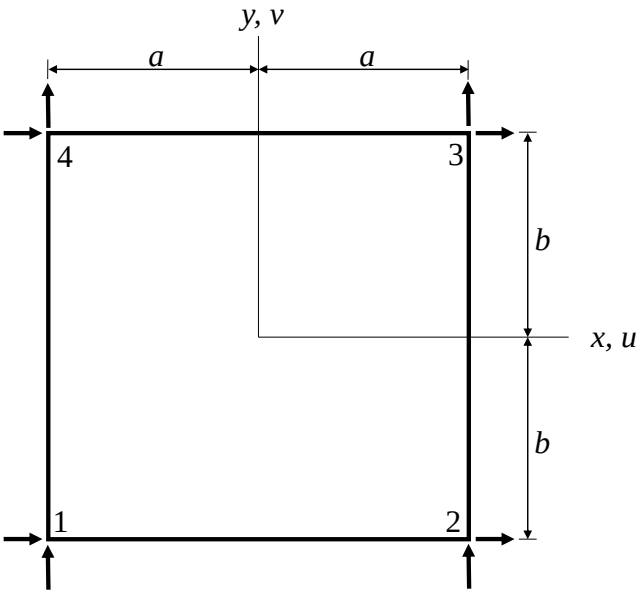

Figure 5.1: Bilinear quadrilateral and its eight nodal d.o.f. (Adapted from Cook *et al.* (2002))

In essence, the chosen response modelling approach should be able to manipulate and populate the matrix of elastic stiffness, **E**.

5.2 Response Modelling using Artificial Neural Networks

The feasibility of using the ANN method of modelling the material response was investigated. The capability of generating a function describing the complex material response changes that occur during multi-cyclic loading was the justification for using this approach.

Preliminary results of modelling the multi-cyclic load-strain response proved troublesome. Describing each individual point in a unique manner so that the combination of those inputs would always lead to the desired output was possible, as shown in Figure 5.2a for normalised values. Input parameters used are shown in Table 5.1, with σ stress, ε strain, and the subscript n referring to the increment number. This method of training the network nurtures a dependence on step size between inputs. When the network is tested on similar data, where only the step size between increments is varied, the effects are detrimental to its capability of predicting the correct strain, shown in Figure 5.2b. The variation in step size during an FE analysis would lead to similar behaviour of the network response.

Table 5.1: Input parameters for ANN modelling of multi-cyclic response

Input No.	Parameter
1	σ_n
2	σ_{n-1}
3	σ_{n-2}
4	ε_{n-1}
5	ε_{n-2}

Modelling the multi-cyclic response of the material has further implications. When a network is trained using data measured during, say, five cycles, the capability of predicting the stress-strain state when the exact load path is not followed cannot be guaranteed. The material response changes continuously during each increment, evident as a steeper gradient of the load path in each succeeding cycle as well as a noticeable amount of permanent deformation at the start of the cycle. This occurrence, along with the unavoidable nurturing of a sensitivity to increment size, necessitates the use of alternative modelling approaches.

Single-cycle data was used to train a network. This much simpler response can uniquely be described using input parameters that will not nurture a sensitivity to increment size. The response of this network in predicting the strain for a load only half that of the maximum it was trained on, was tested for. The response, shown in Figure 5.3, proved unsatisfactory. An inability exists to correct the unload path according to the maximum measured strain

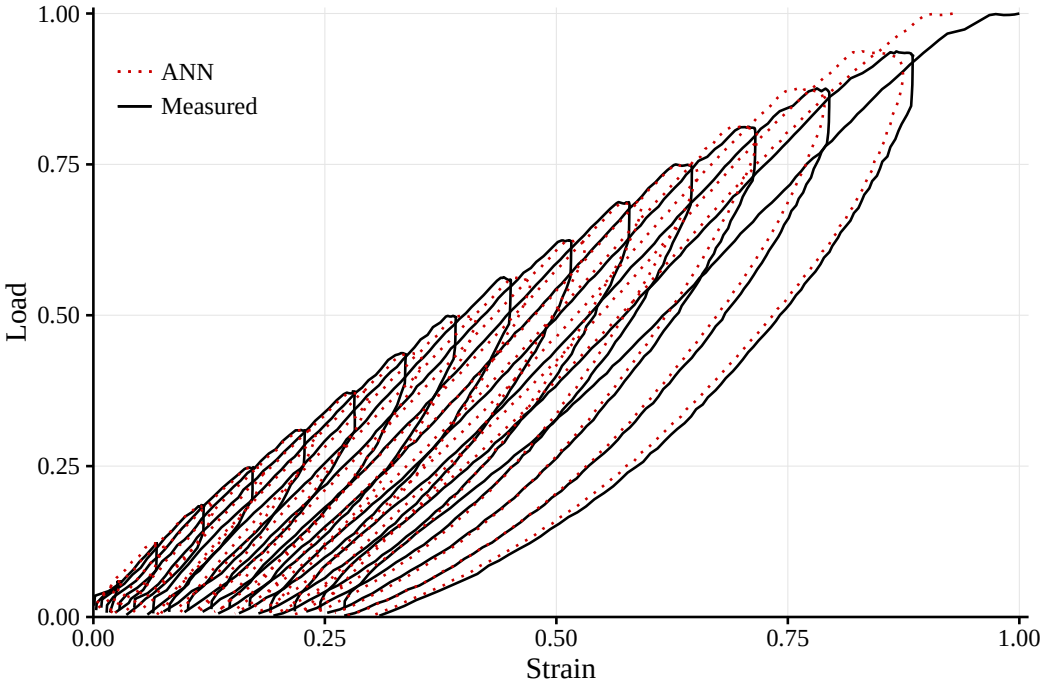

(a) Using similar increment sizes for training and testing results in an overall good prediction capability

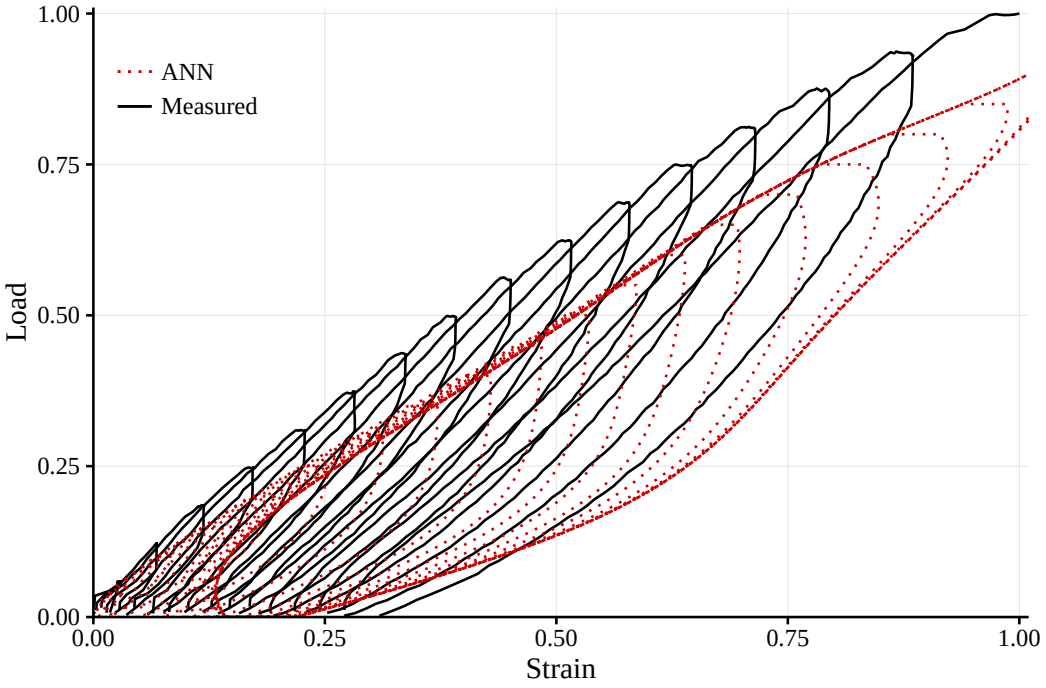

(b) Using dissimilar increment sizes for training and testing brings forth the unwanted nurturing of increment size sensitivity and the subsequent degrading of the networks' prediction capability

Figure 5.2: Sensitivity of ANN to input increment size for modelling multi-cyclic material response, shown only for the material CD and normalised values

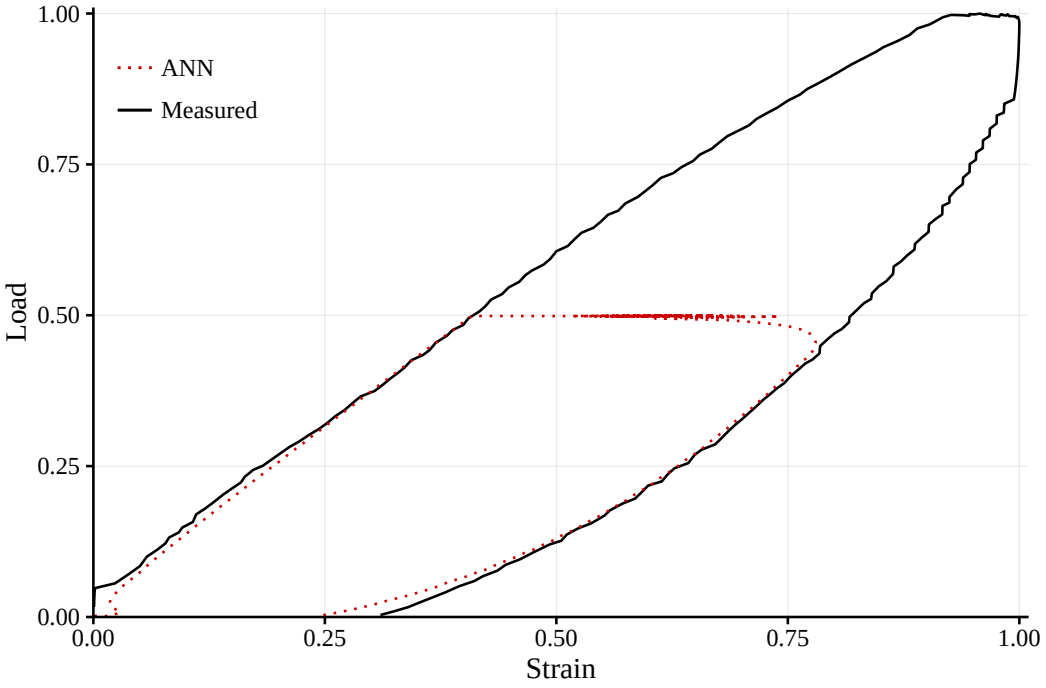

Figure 5.3: Response of ANN to predict strain for half the load that was used during training on full-cycle data

during the test case. Instead, a horizontal leap is made to the unload path on which the network was trained whereafter unloading follows that path.

5.3 Material Response Modelling

The presented response modelling approach utilises data measured during single-cycle tests. The full-cycle response is split to represent the load and unload paths separately. These paths are modelled using two independent functions derived by means of a least squares fit. A model incorporates these functions such that a logical operator is included which can determine whether the material is being loaded or unloaded, and in the case of the latter, adjust the unload path to better represent the measured results gathered during physical testing.

5.3.1 Preparatory Work

The overview of the FE method presented shows that the material model should be capable of populating the elastic stiffness matrix, $\mathbf{E}$. Two response

modelling approaches can be followed to achieve that. The first approach models the stress-strain behaviour directly and then differentiates that with respect to strain, as in Eq. 5.6, to arrive at the stiffness modulus. The second approach calculates the effective stiffness of the measured data and models that as a function of strain.

$$E_t(\varepsilon) = \frac{d\sigma}{d\varepsilon} \tag{5.6}$$

$$E_t(\varepsilon) = \frac{\sigma_n}{\varepsilon_n} \tag{5.7}$$

Preliminary work comparing the two methods against one another showed that the latter approach, where the stiffness modulus is modelled directly in terms of strain, was more accurate. The parameters which dictate the material response are modelled directly accordingly, rather than to the response of those parameters. The loss of information that occurs when the derivative of a function is calculated affects the performance of the former approach. Response modelling is therefore achieved by means of generating functions describing the material stiffness in terms of strain.

The load and unload responses of the material differ vastly, as evident in the results presented in Chapter 4. As such, different methods are used to model these curves.

5.3.2 Load Response

The load response of the material displays different trends in the two material directions. In the CD an exponential trend is evident, whereas the MD better resembles a linear function. These trends were exploited by fitting appropriate functions through the data. The CD is modelled using a power law function as in Eq. 5.8 and the MD a linear function shown in Eq. 5.9. The coefficients β_0 and β_1 are determined by means of a least squares fit.

$$E_{CD}(\varepsilon) = \beta_{0,CD}\varepsilon^{\beta_{1,CD}} \tag{5.8}$$

$$E_{MD}(\varepsilon) = \beta_{0,MD} + \beta_{1,MD}\varepsilon \tag{5.9}$$

This approximated fit, along with the measured response, is shown in Figure 5.4. Upon initial loading the material resists with a low stiffness modulus,

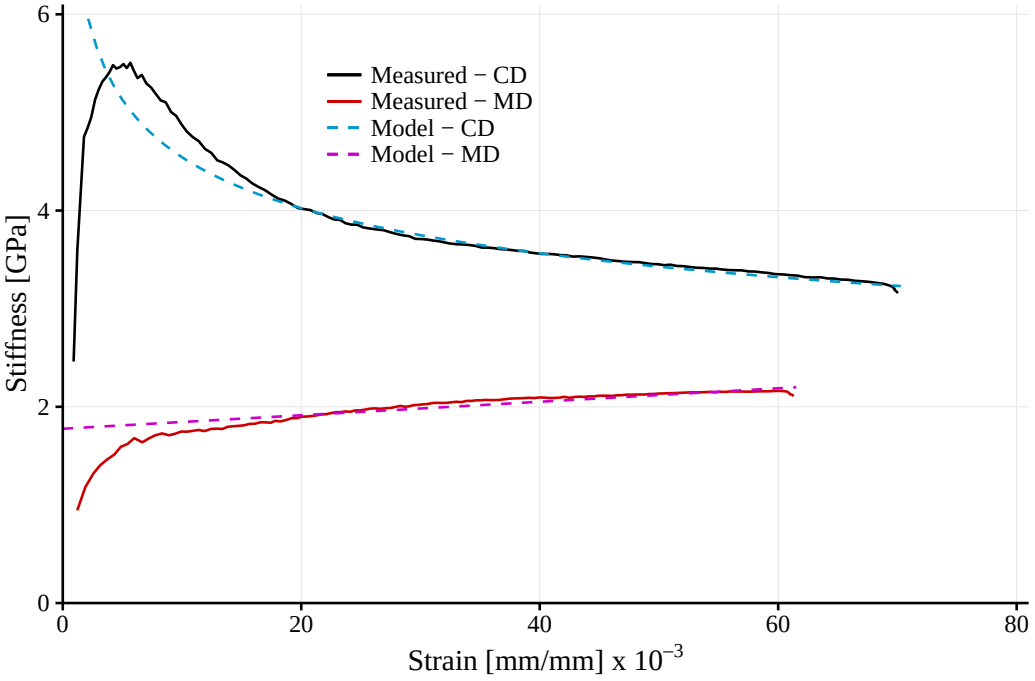

Figure 5.4: Load response model of material stiffness as a function of strain

but as strain increases the modulus follows the exploited trend. The increased interest towards the response at higher strains permits the exclusion thereof upon initial loading.

5.3.3 Unload Response

The unload response of the material is better suited to a linear model of the form in Eq. 5.10. With this model the initial vertical drop cannot be accounted for. However, the strain range in which this drop occurs is very narrow, so merely accounting a difference in the predicted stress between the load and unload models should suffice. The models for both material directions are shown along with measured test data in Figure 5.5.

$$E(\varepsilon) = \beta_2 + \beta_3 \varepsilon \tag{5.10}$$

5.3.4 Combined Response

The presented response modelling approach utilises the two unique functions describing the material load and unload responses. The material stiffness along

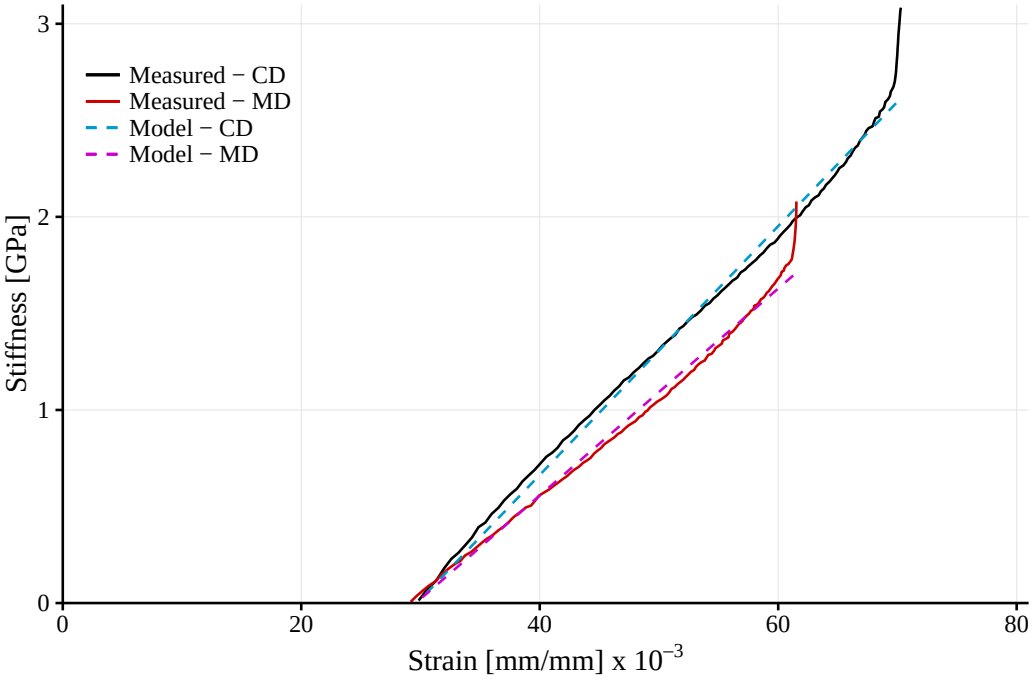

Figure 5.5: Load response model of material stiffness as a function of strain

the load path is calculated using the power law model in Eq. 5.8. The unload response of the material is, however, not as straight forward; the stiffness needs to be compensated for when required for an intermediate load. This adjustment is made as a simultaneous horizontal and vertical shift so that the initial portion of the unload response remains preserved in shape. The details of this process are demonstrated in Eqs. 5.11 to 5.17. It is important to mention that this shifting process must be performed while the model still represents material stiffness. This stiffness value is used to populate the material stiffness matrix of Eq. 5.5, whereafter no interaction with the result can occur. The stiffness should be calculated so that, once multiplied with the vector of strains, the intended result will be produced.

To achieve this bi-directional shift of the response it is necessary for additional parameters in Eq. 5.10. These parameters are used in order to trick the model into calculating the response at a higher strain and then reduce that predicted value with the difference in load between the maximum of the physical test and the maximum of the desired load.

Substituting Eq. 5.11 in to Eq 5.10 to compensate for the difference in strain between that of the maximum in the physical test and the maximum

required for the numerical model

$$\varepsilon = \varepsilon_A + \varepsilon_D \tag{5.11}$$

where ε_A is the actual strain at the current increment and

$$\varepsilon_D = \varepsilon_{T,max} - \varepsilon_{N,max} \tag{5.12}$$

is the difference in strain between the maximum measured on the physical sample, $\varepsilon_{T,max}$, and the maximum measured for that integration point, $\varepsilon_{N,max}$, during the analysis.

Next, the model must be adapted to allow for the stress calculation using only ε_A where it is required for $\varepsilon_A + \varepsilon_D$, as in Eq. 5.13.

$$\sigma_n = \left[\beta_2 + \beta_3(\varepsilon_A + \varepsilon_D)\right](\varepsilon_A + \varepsilon_D) \tag{5.13}$$

To avoid an over-elaborate equation, assign

$$\Upsilon = \left[\beta_2 + \beta_3(\varepsilon_A + \varepsilon_D)\right] \tag{5.14}$$

then

$$\begin{aligned} \sigma_n &= \varepsilon_A \Upsilon + \varepsilon_D \Upsilon \\ &= \varepsilon_A \left[\Upsilon + \frac{\varepsilon_D}{\varepsilon_A}\Upsilon\right] \end{aligned} \tag{5.15}$$

which results in the unload response effectively being shifted horizontally. Hence, stress will be calculated for the correct strain, ε_A, but will result in a too high magnitude. A vertical shift is required, performed as

$$\sigma_n = \varepsilon_A \left[\Upsilon + \frac{\varepsilon_D}{\varepsilon_A}\Upsilon - \frac{\sigma_D}{\varepsilon_A}\right] \tag{5.16}$$

where

$$\sigma_D = \varepsilon_{T,max}\left[\beta_{0,CD}\varepsilon_{T,max}^{\beta_{1,CD}}\right] - \varepsilon_{N,max}\left[\beta_{0,CD}\varepsilon_{N,max}^{\beta_{1,CD}}\right] \tag{5.17}$$

which is the difference in stress between the maximum measured during the physical test and the maximum required for the numerical model at that specific integration point along the load path. For every integration point it is essentially calculated and applied as a constant value.

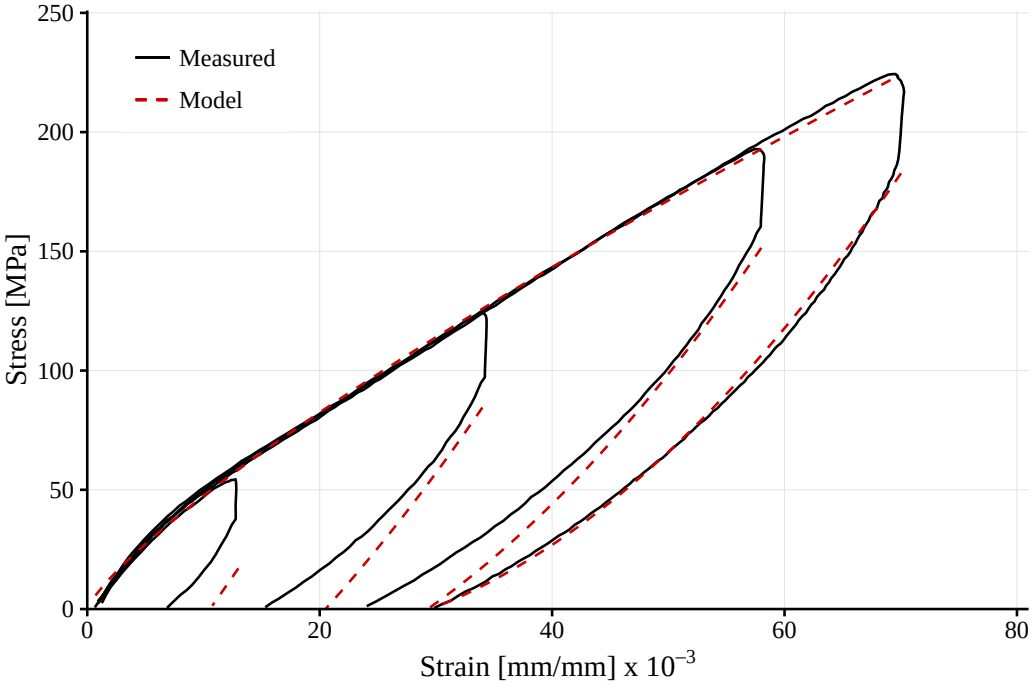

Figure 5.6: Performance of combined response modelling approach in predicting intermediate load paths, for the material CD only

The ability of this modelling approach at predicting stress values along the load and unload paths is demonstrated in Figure 5.6 using the measured data of Figure 4.8. On the load path the model closely matches the measured response with a slight deviation occurring at high strains. The RMS value of the difference between this load model and the measured data is 3.38 MPa. The method of calculating the unload response for three intermediate loads is shown to be accurate. This model best predicts the initial portion of the unload response, which suits the response that would typically be desired from its implementation.

5.3.5 Shear Response and Poisson's Ratio

Response models have only been developed for the tensile behaviour of the material. Shear behaviour and the measurement of Poisson's ratio were outside the scope of the project. However, these properties need to be accounted for during implementation of the material law in the FE environment. For simplicity, Poisson's ratio is set as zero. For isotropic materials with a zero Poisson's ratio, the shear modulus becomes half the elastic modulus. To this

end, for the orthotropic modelling used in this thesis, the average tensile stiffness is calculated and halved as approximation of the shear modulus. An improvement over this method is left as a discussion for further research in Chapter 6.

5.4 Investigation of Numerical Implementation

5.4.1 User-Defined Subroutine

MSC.Marc allows for the implementation of user-defined material laws via subroutines that can be incorporated into analyses. This method directly populates the material stiffness matrix according to the supplied material law, as opposed to the conventional approach which is merely an adjustment of parameters of an existing law. A suitable entry point and base subroutine is a decision made depending on the information required to construct the required material law. The `HYPELA2()` user subroutine was chosen as the base subroutine due to having access to the required variables as standard. Every integration point calls for this routine.

For the presented method, material stiffness is modelled as a function of strain. Two different states of strain need to be captured for every integration point for this purpose: ε^n and $\varepsilon_{N,max}$. The current increments' strain, ε^n, is available in `HYPELA2()` by default. The maximum strain measured during the analysis, $\varepsilon_{N,max}$, is required for both material directions at every integration point. This is not a widely used state and as such cannot be accessed via the standard `HYPELA2()`. Rather, Marc allows users the flexibility to store such information as state variables. Initial conditions of each state variable are set once for all integration points at the beginning of the analysis using the `INITSV()` subroutine. At the end of an increment the updated condition of each state variable is defined within the `NEWSV()` subroutine. This updated state then becomes available to the `HYPELA2()` routine during the following increment when the utility routine `ELMVAR` is called to facilitate its extraction. In total, three state variables are requested from Marc, where the first is always reserved for temperature, shown in Table 5.2.

The response models exhibit a discontinuity at the switch-over point be-

Table 5.2: State variables used for Marc subroutine implementation

No.	1	2	3
SV	Temperature	$\varepsilon_{CD,max}$	$\varepsilon_{MD,max}$

tween the load- and unload model. To assist with convergence in the FE model, `HYPELA2()` allows for the updated stress to be calculated within the subroutine using the newly formed material stiffness matrix and the current strain increment.

The complete Fortran code implementing all three subroutines for describing the user-defined material law is presented in Appendix B.

5.4.2 Initial Performance Evaluation

The initial model describing the full load-unload cycle was tested for using a single membrane element test case. This allowed full control over all four integration points, aiding with the problem-finding phase. Geometries were subsequently tested for using an increased amount of square elements along with loading schemes such as uniaxial tension and biaxial tension. A demonstration of the material law in predicting the full load-unload path of the FE model loaded to a maximum strain equivalent to that of the physical test is shown in Figure 5.7 for both material directions. The capability of the material law to estimate the unload path for intermediate loads is shown along with results from physical testing in Figure 5.8 for the material CD. The four element test case in Figure 5.9 describes the loads and boundary conditions.

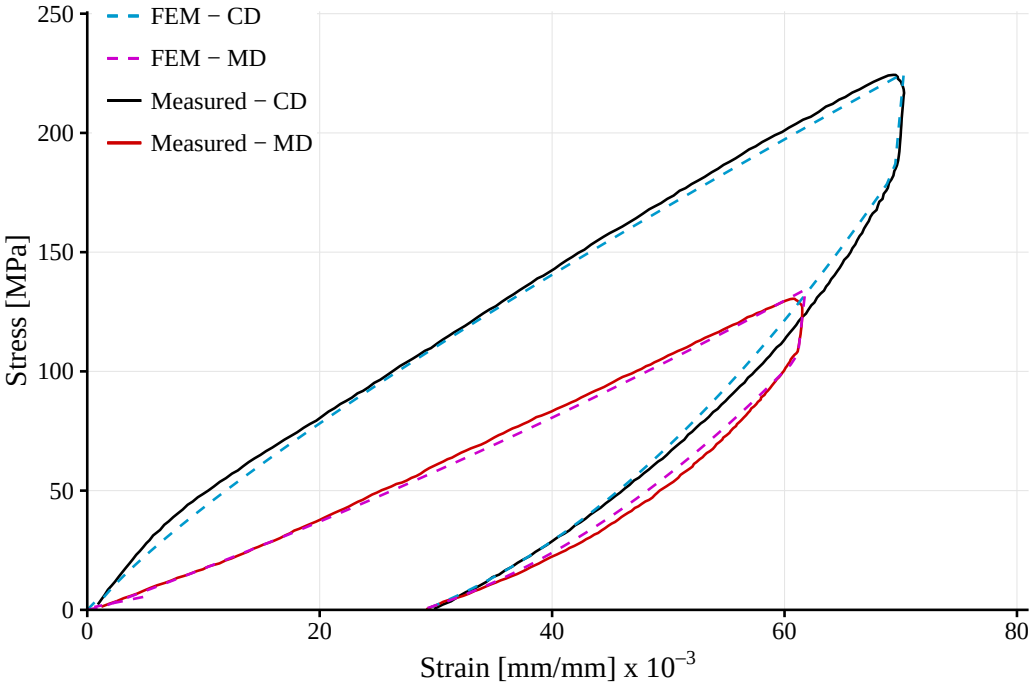

Figure 5.7: Performance of user-defined material law implemented in MSC.Marc compared to physical test results for both material directions

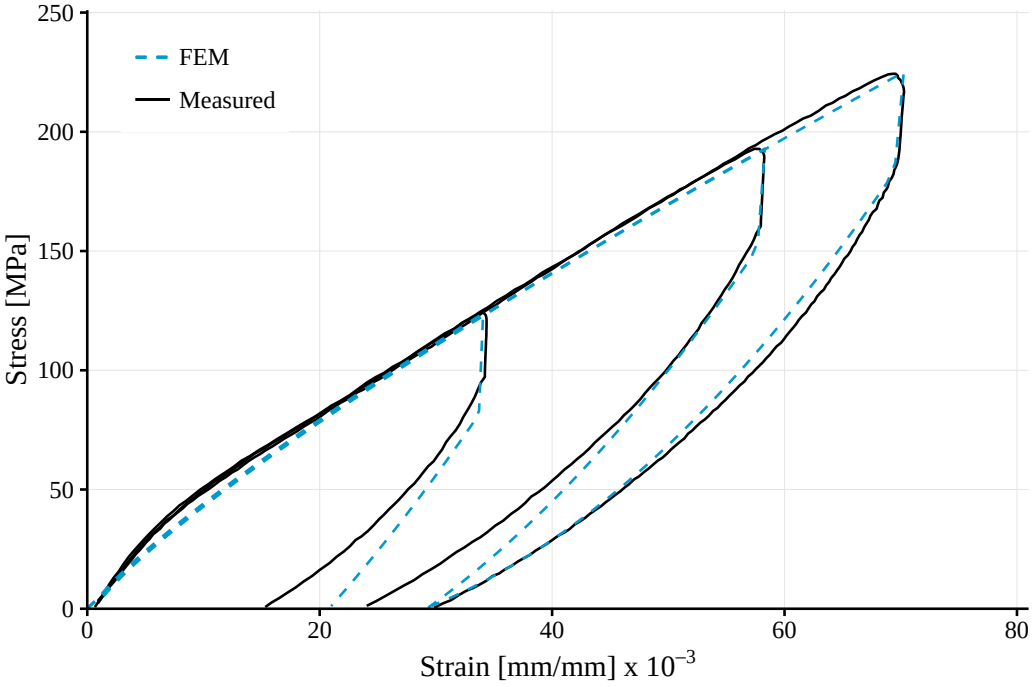

Figure 5.8: Performance of user-defined material law implemented in MSC.Marc compared to physical test results for material CD and intermediate loading

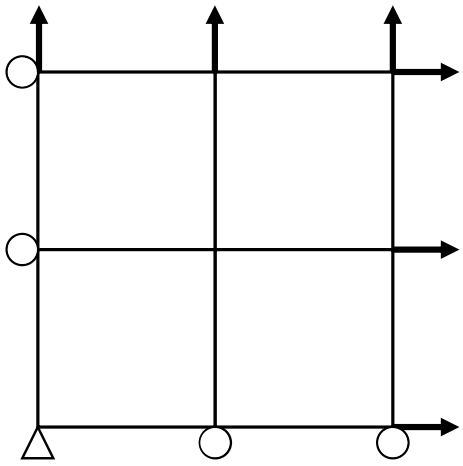

Figure 5.9: Loads and boundary conditions of four element test case used for Figures 5.7 and 5.8

Chapter 6

Concluding Remarks and Recommendations

A method for measuring and characterising the mechanical response of woven polypropylene at the fabric level was explored. This response model was used during an initial investigation into the implementation as part of a Finite Element (FE) analysis, ultimately demonstrating the intended application thereof as well as its feasibility as a working foundation on which to base further numerical developments.

6.1 Performance of BASR

The lack of a means to easily cater for repeated biaxial tension testing of the woven polypropylene was dealt with the development of the Biaxial and Shear Rig (BASR). This rig allowed short turn-around times between subsequent tests, ultimately assisting in performing a larger number of tests. The wide array of commissioning tests that was conducted showed that the performance of the simple control system was sufficient for the rates at which the load-controlled tests were run. Further, the linear equation relating the measured voltage signal from the pressure transducer to that of force can be used for the full 4000 N range it was calibrated on.

Uniaxial tensile testing of aluminium samples incorporated multiple facets of the test rig. The near perfect-plastic regime inherent to the material aided in establishing a sufficient degree of strain rate control. It was shown that accurate and repeatable material properties could be measured using the BASR

when compared directly to the ASTM E8M standard for testing metallic materials using the MTS Criterion test rig. The independent control of the two biaxial directions and the performance evaluation of each of those directions for uniaxial tensile testing is a sufficient indication to its ability at testing polymers.

6.2 Mechanical Testing of Woven Polypropylene

A load case was designed to test for the desired mechanical response of woven polypropylene using a single-cycle to maximum applied load. Effects related to a time-dependent characteristic of the material were established to be stemming from creep. Sustained maximum load over an extended time period was avoided to mitigate this effect. The cyclic nature of the load path was shown to not greatly influence the form of the load-strain response and allowed for less time-consuming single-cycle testing to be performed over that of a multi-cyclic approach. The coupled response between orthogonal material directions was tested using five different load ratios and found not to be as pronounced as for certain variations of the material found in literature.

6.3 Regression Modelling of Material Response

Using an Artificial Neural Network to model material response was investigated and the limitations thereof used as leverage to justify the much simpler method of using regression modelling. Material response is calculated and modelled as the immediate material stiffness. The load response of the material CD is approximated using a power law equation, and the load response of the material MD, as well as that for unload of both directions, using linear fits. To compensate for using the unload response measured from a high force magnitude an equation was derived that shifts the response thereof according to the load required. This regression model proved sufficiently accurate at capturing the full load response of the material. The unload response to three different intermediate loads showed that the initial portion is approximated

closely whereafter the prediction degrades. The lowest intermediate load was approximated poorly. This poor prediction demonstrates the importance of performing physical testing in the range where the response is desired.

6.4 Investigation of Numerical Implementation

The intended application of the response model was demonstrated initially by coding it as the user-defined material law in a Fortran subroutine for implementation in MSC.Marc. Preliminary work indicates that such an approach of directly modelling material stiffness as a function of strain can be used to populate the material stiffness matrix within the FE environment. Further, the discontinuity that exists between the model for load response and the model for unload response can be solved using the `HYPELA2()` subroutine in Marc by calculating the predicted stress for each increment. The ability of the subroutine to correctly calculate the unload path for two intermediate full load paths was shown to be as accurate as the response model alone.

6.5 Significant Contributions

A summary of the various contributions made for a simplified approach at testing and modelling woven polypropylene are shown:

1. Developed a biaxial and shear test rig capable of testing a variety of materials and load ratios.

2. Formulated a method of using physical data from a single-cycle test to model the full load-unload response for loads intermediate to that tested for.

3. Showed the possibility of supplying the response model as a material law in a user-defined subroutine for numerical analysis in commercial software and demonstrated its ability at predicting intermediate unload paths.

6.6 Future Recommendations

This thesis only performed preliminary work on the numerical implementation of the response model. Further research into the details of this promising technique can be done to improve the generalisation thereof to arbitrary element geometries and loading schemes. A suitable test would be a Patch Test which is used to establish whether an assembly of elements can display a constant state of strain. Passing this test is a necessary condition to show that computed results will converge towards exact results during mesh refinement.

The method of testing for the shear response of the material did not fall within the scope of this project. However, the designed test rig does allow for the testing thereof. Future work should include commissioning that functionality of the rig.

Polymers are known to exhibit a significant amount of creep even at room temperatures. The developed test rig can be used to test for this response to be incorporated into a response model.

Shear behaviour of the material was approximated using the average of the two tensile stiffness moduli. An increase in accuracy can potentially be achieved if the shear stiffness is calculated and modelled in a similar fashion as for the tensile response.

Appendices

Appendix A

Experimental Setup and Procedure

Details of the steps followed to ensure repeatability amongst samples and tests are detailed within this Appendix.

A.1 Sample Preparation

1. Source material from reputable manufacturer to ensure quality of product.
2. Lay material on flat surface and outline the cruciform to the dimensions in Figure A.1. The packing arrangement in Figure A.2 can be used to reduce material wastage and the total distance of cutting required.
3. Cut along marked lines parallel to tows in the specific material direction.
4. Number samples individually.
5. Remove two tows from each side of the cruciform.
6. Mechanically precondition sample.
7. Mask off central area of interest and apply contrasting speckle pattern.
8. Store on a flat surface away from direct sunlight under similar environmental conditions under which physical testing will be performed for a period of 24 hours prior to the test.

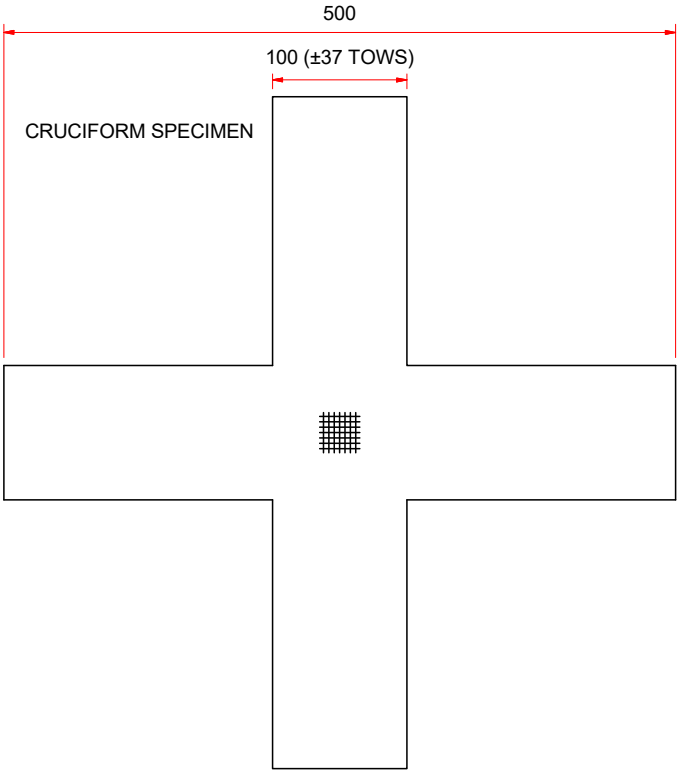

Figure A.1: Required dimensions for polypropylene specimen

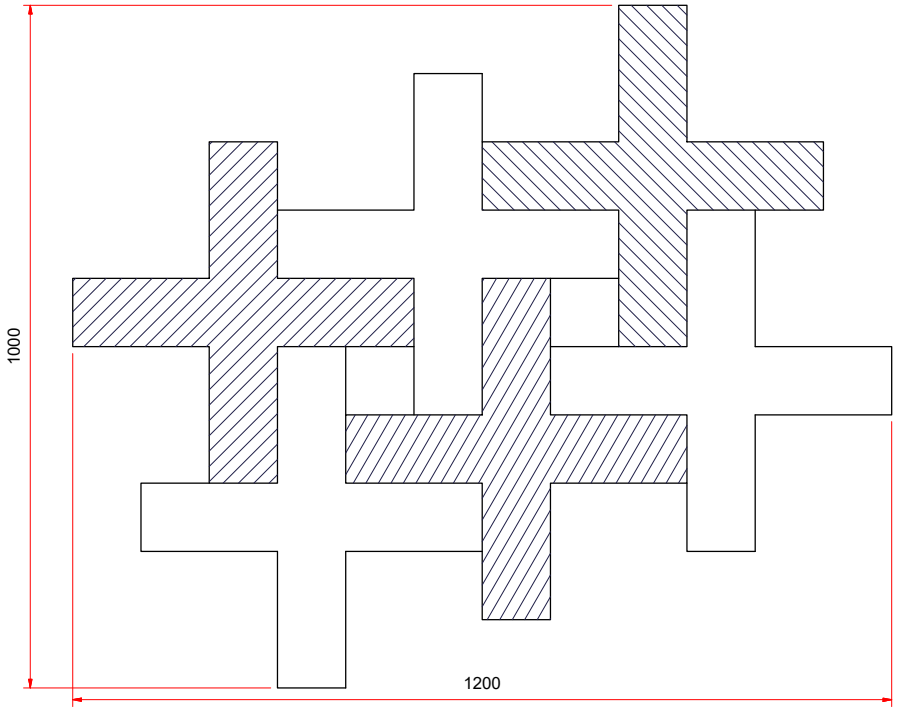

Figure A.2: Packing arrangement

A.2 Hardware Setup

The set up procedure for the hardware required for biaxial testing using the DIC needs to be performed before each testing session. The procedure is as follows:

1. Cordon off testing area around the BASR using danger tape.
2. Ensure that the moving parts of the BASR are lubricated sufficiently and are in general working condition.
3. Insert material cruciform to assist with initial set up.
4. Electrically connect Festo MPPES pneumatic pressure regulators to the National Instruments USB DAQ.
5. Momentarily load cruciform to 200 N whereafter the load should be released.
6. Position tripod so that the attached beam overhangs directly above the testing area of the BASR at a height of 520 mm, measured from the top of the cruciform to the tip of the camera lense.
7. Ensure tripod is stable to small perturbations.
8. Attach the two E-lite cameras and programmable timing unit (PTU) to overhanging beam and connect them to the Dell laptop running the DaVis software.
9. Focus the cameras on the inserted cruciform so that the central area of interest fills the image. This is achieved by adjusting the overall height of the tripod and the focal length of the camera lense. Ensure sufficient ambient light is available to alleviate the use of the additional LED lighting.
10. Set camera exposure to 4000 µs
11. Calibrate the cameras using the 058-5 calibration plate, placed on top of the inserted cruciform. The average position error should be less than 0.5 pixels.

Figure A.3: BASR and DIC hardware required for experimental testing during the setup procedure

12. Set capture frequency to 2 Hz

13. Perform a dry-run test to a maximum load of 500 N in the CD and 250 N in the MD. Ensure the pressure measurements are in agreement with the subjected load.

Figure A.3 shows the hardware during the experimental setup.

A.3 Test Procedure

1. Testing should take place at night such that the changing environmental lighting cannot affect calibration. Instead, rely solely on artificial fluorescent tubes.

2. Ensure all pneumatic cylinders are fully extended.

3. Set material grips to the centre.

4. Insert cruciform.

5. Load sample to 200 N for 30 s.

6. While sample is loaded ensure that all wrinkles have dissipated.

7. Remove load.
8. Ensure sample is within the viewing area of the DIC cameras.
9. Select required load case and input desired maximum loads.
10. Perform required test.
11. Remove sample.

Appendix B

User-Defined Fortran Subroutine

```
!HYPELA2() subroutine
! User subroutine to input user-defined material law
!A line to check that no code exceeds after column 73 which will be cut!
      subroutine hypela2(d,g,e,de,s,t,dt,ngens,m,nn,kcus,matus,ndi,
     2 nshear,disp,dispt,coord,ffn,frotn,strechn,eigvn,ffn1,frotn1,
     3 strechn1,eigvn1,ncrd,itel,ndeg,ndm,nnode,
     4 jtype,lclass,ifr,ifu)
!
#ifdef _IMPLICITNONE
      implicit none
#else
      implicit logical (a-z)
#endif
!
! **********   Start of generated type statements  **********
      real*8 coord, d, de, dt, disp, dispt
      real*8 e, eigvn, eigvn1, m, kcus, matus, ndi
      real*8 ffn, ffn1, frotn, frotn1, g, nnode, jtype
      real*8 s, strechn, strechn1, t, lclass, dum1, det
      integer i, ifr, ifu, itel, ncrd, ndeg, ndm, nn, ngens
      integer nshear
      real*8 b0CD, b1CD, b0MD, b1MD
      real*8 b2CD, b3CD, b2MD, b3MD
      real*8 E1, E2, G12, Ex, Ey, Gxy
      real*8 epsdiff, ups, sigdiff, maxex, maxey
      real*8 eCD, eMD, s0
```

```
27        dimension e(3),de(3),g(3),d(ngens,ngens), s(3), s0(3), disp(3)
28  !
29  ! *************   Inputs used from subroutine  ************************
30  !     d             stress strain law to be formed
31  !
32  !     e             total strain
33  !
34  !     de            increment of strain
35  !
36  !     s             stress
37  !
38  !     t             state variables
39  !
40  !     dt            increment of state variables
41  !
42  !     ngens         size of stress - strain law
43  !
44  !     ndi           number of direct components
45  !
46  !     t             is the state variables at the
47  !                    beginning of the increment.
48  !                    t(2) max x-component of strain
49  !                    t(3) max y-component of strain
50  ! ********************************************************************
51  !
52  !  Maximum strain values of physical test data
53        eCD=0.07028679d0
54        eMD=0.06152376d0
55  !
56  !  Coefficients of response power law function (Load - Cross direction)
57        b0CD=21.4314996d0
58        b1CD=-0.1748921d0
59  !  Coefficients of response linear function (Unload - Cross direction)
60        b2CD=-1913701138d0
61        b3CD=64427755896d0
62  !
63  !  Coefficients of response linear function (Load - Machine direction)
64        b0MD=1776437627d0
65        b1MD=6870387464d0
66  !  Coefficients of response linear function (Unload - Machine direction)
67        b2MD=-1587215033d0
68        b3MD=53604726402d0
```

```
!
!  Initialize both stiffness parameters as zero
      E1=0
      E2=0
!
!  Call the second SV, max strain in x-direction
      call elmvar(29,m,nn,kcus,maxex)
!  Call the third SV, max strain in y-direction
      call elmvar(39,m,nn,kcus,maxey)
!
!  Determine whether load is increasing or decreasing in
!  x-direction
!  If strain is positive
      if (e(1) .GT. 0) then
!  If increasing
      if (de(1) .GE. 0) then
!  Calculate stiffness values using power law function
      E1=exp(b0CD)*(e(1))**b1CD
!  Apply upper boundary to stiffness (Power law tends to infinity)
      if (e(1) .LE. 1e-4) then
       E1=10.e9
      end if
      end if
!
!  If decreasing:
      if (de(1) .LT. 0) then
!  Calculate stiffness values using linear function with logic
      if (maxex .LE. 6e-3) then
!  Response model degrades at low strains - adjust to supress
!    numerical instability
      E1=1.e9
      else
!  Eq. 5.12
      epsdiff=eCD-maxex
!  Eq. 5.14
      ups=b2CD+b3CD*(e(1)+epsdiff)
!  Eq. 5.17
      sigdiff=eCD*(exp(b0CD)*(eCD)**b1CD)-
     *          maxex*(exp(b0CD)*(maxex)**b1CD)
!  Eq. 5.16
      E1=ups+(epsdiff/e(1))*ups-(sigdiff/e(1))
!
```

```
111       end if
112       end if
113       end if
114 !
115 !  y-direction
116 !  If strain is positive
117       if (e(2) .GT. 0) then
118 !  If increasing
119       if (de(2) .GE. 0) then
120 !  Calculate stiffness values using linear function
121       E2=(b0MD)+(e(2))*b1MD
122       end if
123 !
124 !  If decreasing:
125       if (de(2) .LT. 0) then
126 !  Calculate stiffness values using linear function with logic
127       if (e(2) .LE. 6e-3) then
128 !  Response model degrades at low strains - adjust to supress
129 !    numerical instability
130       E2=1.e9
131       else
132 !  Eq. 5.12
133       epsdiff=eMD-maxey
134 !  Eq. 5.14
135       ups=b2MD+b3MD*(e(2)+epsdiff)
136 !  Eq. 5.17
137       sigdiff=eMD*((b0MD)+(eMD)*b1MD)-
138      *          maxey*((b0MD)+(maxey)*b1MD)
139 !  Eq. 5.16
140       E2=ups+(epsdiff/e(2))*ups-(sigdiff/e(2))
141       end if
142       end if
143       end if
144 !
145 ! These factors suppress numerical instability
146       if (E1 .LT. 0) then
147        E1=-1.e9
148       end if
149 !
150       if (E2 .LT. 0) then
151       E2=-1.e9
152       end if
```

```
153 !
154       if (E1 .EQ. 0) then
155        E1=5.e9
156       end if
157 !
158       if (E2 .EQ. 0) then
159       E2=1.e9
160       end if
161 !
162       G12=(E1+E2)/4.d0
163 !  Modified for orthotropic material
164       Ex=E1
165       Ey=E2
166       Gxy=G12
167 !  b-matrix for membrane elements (Element No. 18)
168 !  Strain-stress matrix
169       d(1,1)=Ex
170       d(2,2)=Ey
171       d(3,3)=Gxy
172       d(2,1)=0
173       d(3,2)=0
174       d(1,3)=0
175       d(3,1)=d(1,3)
176       d(1,2)=d(2,1)
177       d(2,3)=d(3,2)
178 !
179 !  Updated stresses
180       call gmprd (d,e,s,3,3,1)
181 !
182       return
183       end
184 !
185 !
186 !INITSV() subroutine
187 ! User subroutine to input initial values of state variables
188       subroutine initsv(sv,layers,intpts,m,id)
189 #ifdef _IMPLICITNONE
190       implicit none
191 #else
192       implicit logical (a-z)
193 #endif
194       integer id, intpts, layers, m, ii
```

```
195       real*8 sv
196       dimension sv(layers,intpts)
197 !
198 ! *************   Inputs used from subroutine  ************************
199 !     sv             the array of new values for state variable
200 !
201 !     intpts         number of integration points in the element
202 ! ********************************************************************
203 !
204       do ii=1,intpts
205         sv(1,ii)=0.0d0
206       end do
207       return
208       end
209 !
210 !
211 !NEWSV() subroutine
212 ! User routine for updating state variables
213       subroutine newsv(sv,layers,intpts,m,id)
214 #ifdef _IMPLICITNONE
215       implicit none
216 #else
217       implicit logical (a-z)
218 #endif
219       include "lass.cmn"
220       include "dimen.cmn"
221       include "space.cmn"
222       include "heat.cmn"
223       include "array4.cmn"
224       integer id, intpts, layers, m, icode, ii
225       real*8 sv
226       real*8 maxex, maxey, prex, prey
227       dimension sv(layers,intpts)
228 !
229 ! *************   Inputs used from subroutine  ************************
230 !     sv          is the array of new values of this state variable;
231 !                 to be defined by you.
232 !
233 !     intpts      is the number of integration points in this element.
234 !
235 !     m           is the user element number.
236 !                 the internal element number is obtained as
```

```
237 !                  mint=ielint(m).
238 !
239 !     id          is the state variable number as defined in the input.
240 !
241 !     icode       is the standard post code. Obtained in the model
242 !                 definition section in the POST option of Marc Volume C.
243 !
244 !     kcus        is the internal layer number.
245 ! ******************************************************************
246 !
247 ! Updating SV for maximum strain in:
248 ! x-direction (Material CD)
249       if (id .EQ. 2) then
250         do ii=1,intpts
251 ! 1 for x-strain
252           call elmvar(1,m,ii,kcus,prex)
253 ! 29 for total value of second state variable
254           call elmvar(29,m,ii,kcus,maxex)
255           if(maxex .LT. prex) then
256             maxex=prex
257           end if
258           sv(1,ii)=maxex
259         end do
260       end if
261 ! y-direction (Material MD)
262       if (id .EQ. 3) then
263       icode=2
264         do ii=1,intpts
265 ! 2 for y-strain
266           call elmvar(2,m,ii,kcus,prey)
267 ! 39 for total value of second state variable
268           call elmvar(39,m,ii,kcus,maxey)
269           if(maxey .LT. prey) then
270             maxey=prey
271           end if
272           sv(1,ii)=maxey
273         end do
274       end if
275       return
276       end
277 ! ******************************************************************
```

Appendix C

Machine Drawings of BASR

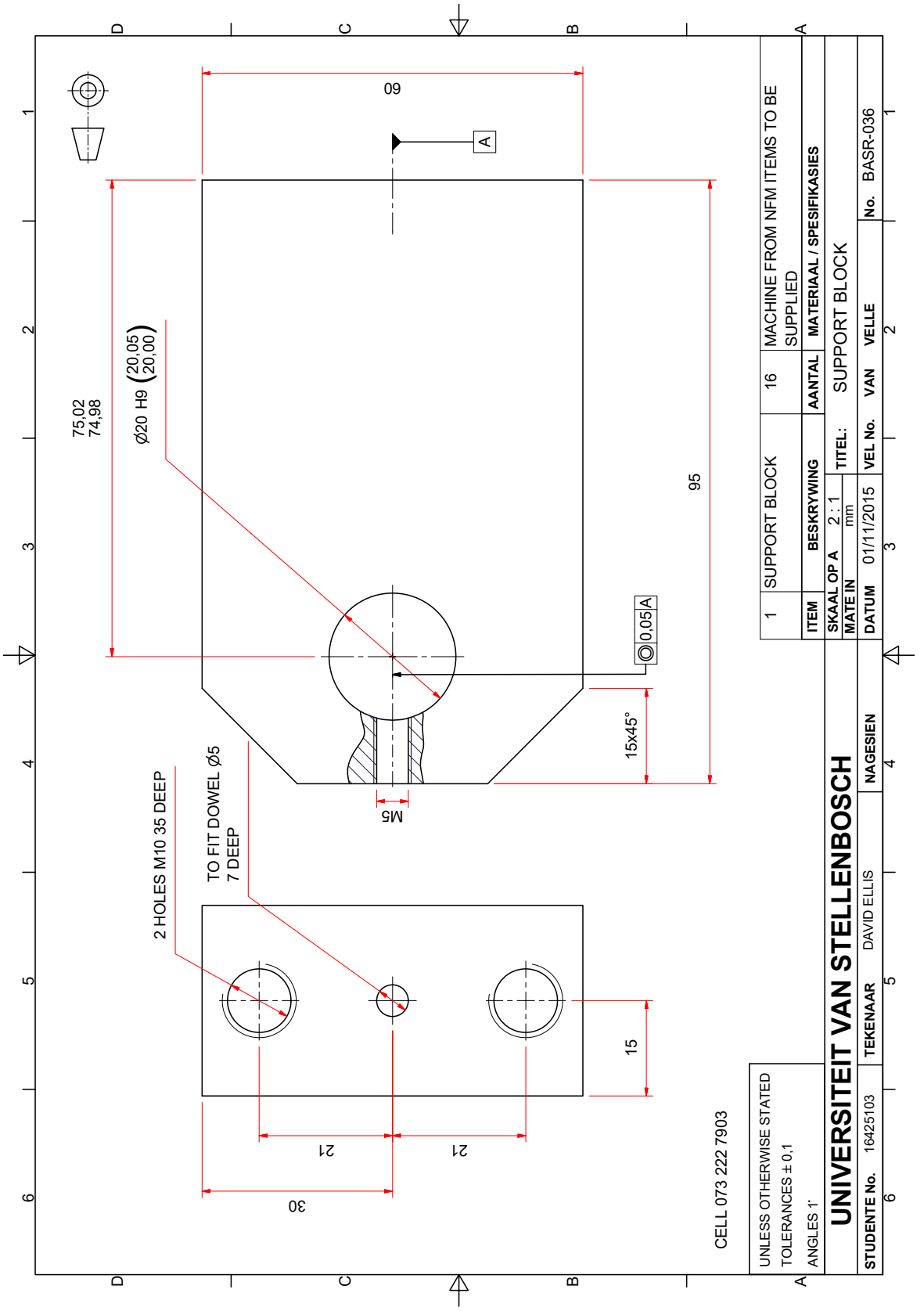

Figure C.1: Aluminium support block for hardened steel guide shaft

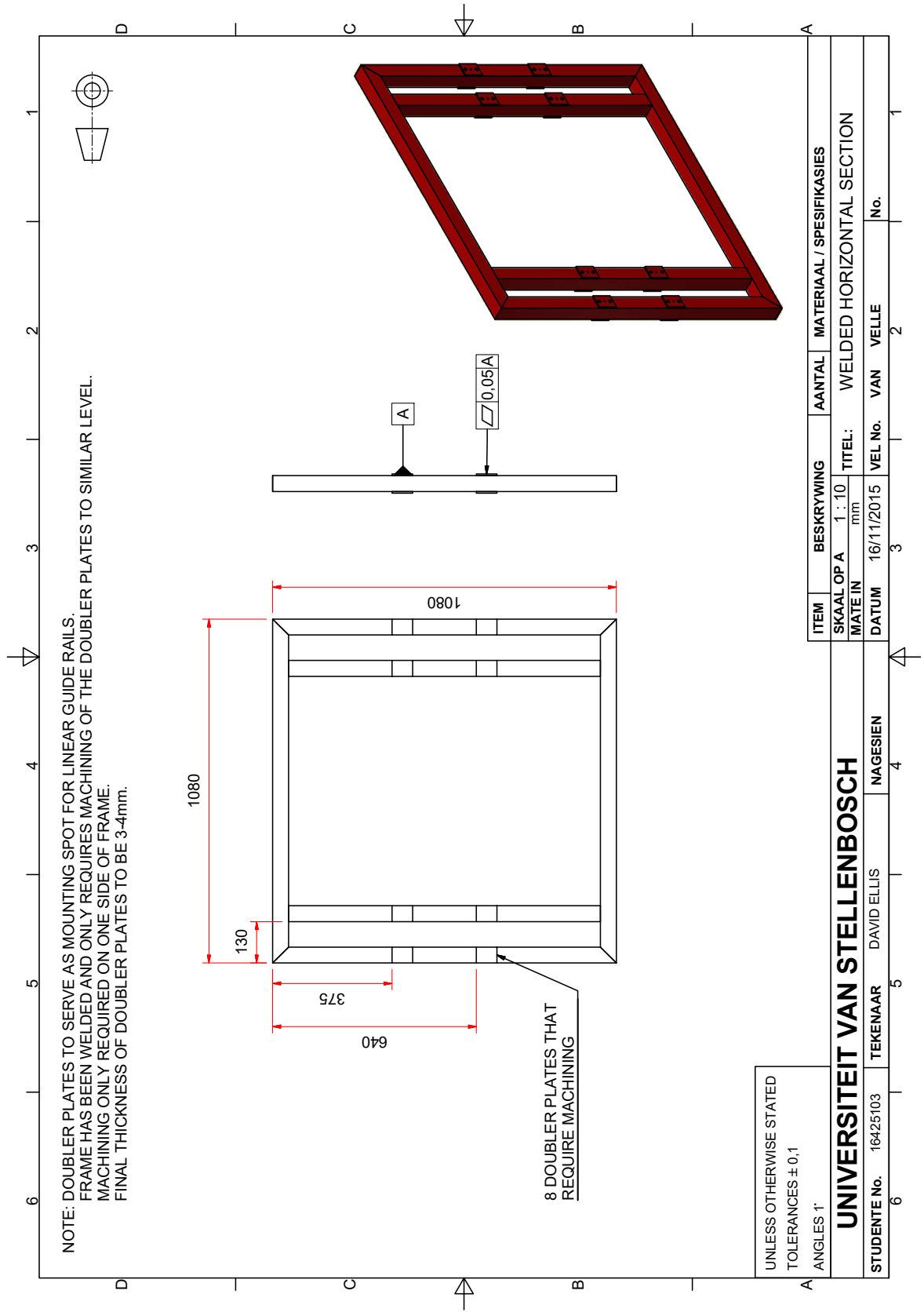

Figure C.2: Required machining of doubler plates to which aluminium support blocks are fastened to ensure the geometric tolerance of flatness is met

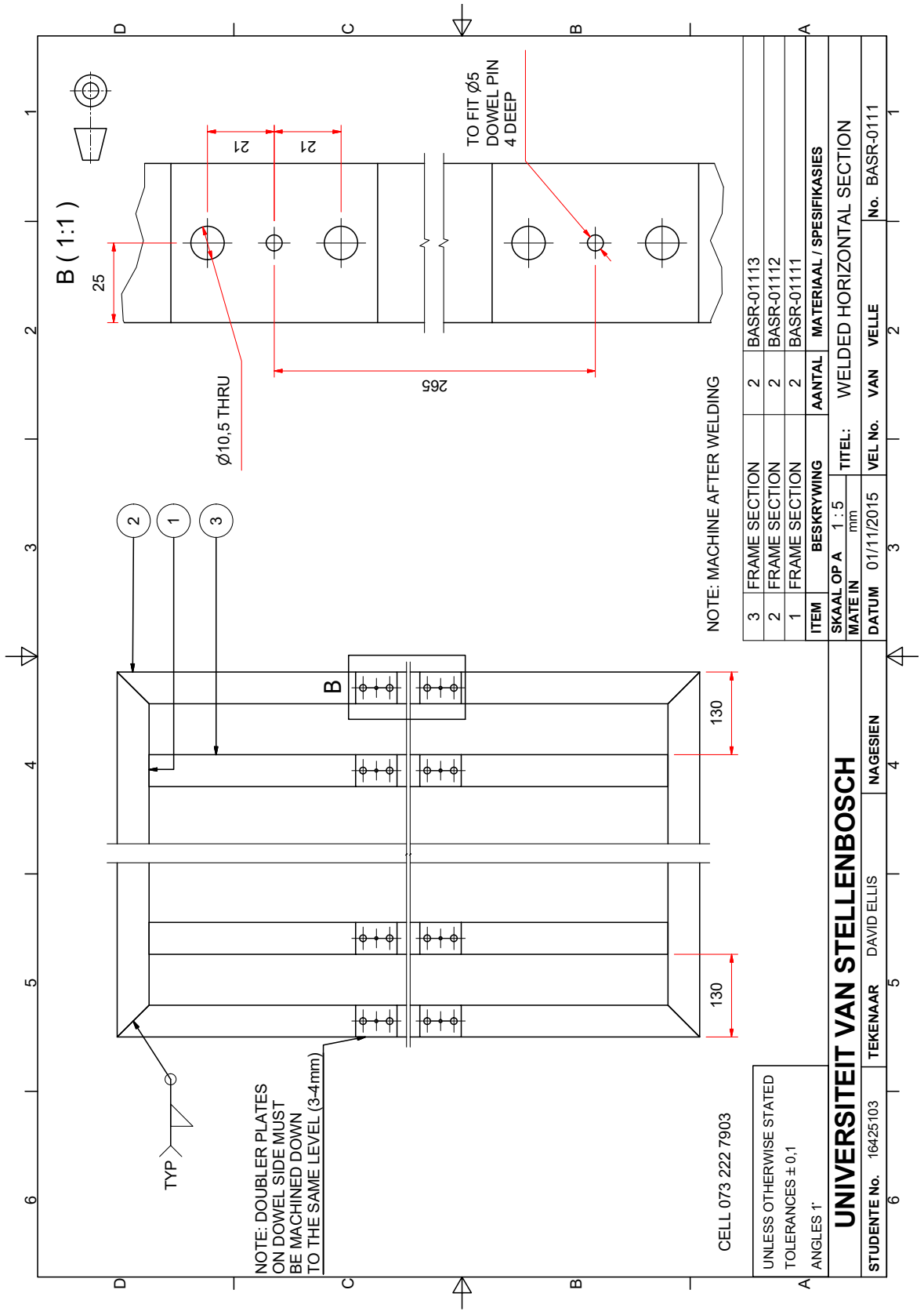

Figure C.3: Required machining of doubler plates to which aluminium support blocks are fastened for positional placement.

List of References

Adumitroaie, A. and Barbero, E. (2011). Beyond plain weave fabrics II. Mechanical properties. *Composite Structures*, vol. 93, no. 5, pp. 1449–1462.

Bergstrom, J. (1999). *Large Strain Time-Dependent Behaviour of Elastomeric Materials*. PhD Dissertation, Massachusettes Institute of Technology.

Boisse, P., Borr, M., Buet, K. and Cherouat, A. (1997). Finite element simulations of textile composite forming including the biaxial fabric behaviour. *Composites Part B: Engineering*, vol. 28, no. 4, pp. 453–464.

Cao, J., Akkerman, R., Boisse, P., Chen, J., Cheng, H.S., de Graaf, E.F., Gorczyca, J.L., Harrison, P., Hivet, G., Launay, J., Lee, W., Liu, L., Lomov, S., Long, A., de Luycker, E., Morestin, F., Padvoiskis, J., Peng, X.Q., Sherwood, J., Stoilova, T., Tao, X.M., Verpoest, I., Willems, A., Wiggers, J., Yu, T.X. and Zhu, B. (2008). Characterization of mechanical behavior of woven fabrics: Experimental methods and benchmark results. *Composites Part A: Applied Science and Manufacturing*, vol. 39, pp. 1037–1053.

Cavallaro, P., Johnson, M. and Sadegh, A. (2003). Mechanics of plain-woven fabrics for inflated structures. *Composite Structures*, vol. 61, no. 4, pp. 375–393.

Cavallaro, P., Sadegh, A. and Quigley, C. (2007). Decrimping behavior of uncoated plain-woven fabrics subjected to combined biaxial tension and shear stresses. *Textile Research Journal*, vol. 77, no. 6, pp. 403–416.

Chen, W., Gao, C., Zhang, D. and Gong, J. (2015). Shear test method of architectural coated-fabrics subjected to biaxial tensile loading. *International Conference on Textile Composites and Inflatable Structures*, vol. 7, no. 8, pp. 544–554.

Cook, R., Malkus, D., Plesha, M. and Witt, R. (2002). *Concepts and Applications of Finite Element Analysis*. 4th Ed. John Wiley and Sons, Inc.

Crammond, G., Boyd, S. and Dulieu-Barton, J. (2013). Speckle pattern quality assessment for digital image correlation. *Optics and Lasers in Engineering*, vol. 51, no. 12, pp. 1368–1378.

Farboodmanesh, S., Chen, J., Mead, J. and White, K. (2006). Effect of Construction on Mechanical Behavior of Fabric Reinforced Rubber. *Rubber Chemistry and Technology*, vol. 79, no. 2, pp. 199–216.

Furukawa, T. and Yagawa, G. (1998). Implicit Constitutive Modelling for Viscoplasticity Using Neural Networks. *International Journal for Numerical Methods in Engineering*, vol. 43, pp. 195–219.

Galliot, C. and Luchsinger, R. (2010*a*). The shear ramp: A new test method for the investigation of coated fabric shear behaviour Part I: Theory. *Composites Part A: Applied Science and Manufacturing*, vol. 41, no. 12, pp. 1743–1749.

Galliot, C. and Luchsinger, R. (2010*b*). The shear ramp: A new test method for the investigation of coated fabric shear behaviour Part II: Experimental validation. *Composites Part A: Applied Science and Manufacturing*, vol. 41, no. 12, pp. 1750–1759.

Ghaboussi, J., Garret, J. and Wu, X. (1991). Knowledge-Based Modelling of Material Behaviour with Neural Networks. *Journal of Engineering Mechanics*, vol. 117, no. 1, pp. 132–153.

Ghaboussi, J., Wu, X. and Kaklauskas, G. (1999). *Neural Network Material Modelling*. PhD.

Grujicic, M., Bell, W.C., Arakere, G., He, T. and Cheeseman, B.A. (2009). A meso-scale unit-cell based material model for the single-ply flexible-fabric armor. *Materials and Design*, vol. 30, no. 9, pp. 3690–3704.

Hashash, Y.M., Jung, S. and Ghaboussi, J. (2004). Numerical implementation of a neural network based material model in finite element analysis. *International Journal for Numerical Methods in Engineering*, vol. 59, no. 7, pp. 989–1005.

Hearle, J., Grosberg, P. and Backer, S. (1969). *Structural mechanics of fibers, yarns, and fabrics*. No. v. 1 in Structural Mechanics of Fibers, Yarns, and Fabrics. Wiley-Interscience.

Hu, J. (2004). *Structure and Mechanics of Woven Fabrics*. Woodhead Publishing Limited, Cambridge England.

Ivanov, D., Ivanov, S., Lomov, S. and Verpoest, I. (2009). Strain mapping analysis of textile composites. *Optics and Lasers in Engineering*, vol. 47, pp. 360–370.

Javadi, A., Mehravar, M., Faramarzi, A. and Ahangar-Asr, A. (2009). An Artificial Intelligence Based Finite Element Method. *Computers and Intelligent Systems*, vol. 1, no. 2.

Jung, S. and Ghaboussi, J. (2006). Neural network constitutive model for rate-dependent materials. *Computers & Structures*, vol. 84, no. 15-16, pp. 955–963.

King, M. and Socrate, S. (2004). *ASME 2004 International Mechanical Engineering Congress and Exposition*.

King, M.J., Jearanaisilawong, P. and Socrate, S. (2005). A continuum constitutive model for the mechanical behavior of woven fabrics. *International Journal of Solids and Structures*, vol. 42, pp. 3867–3896.

LaVision GmbH (2014). *Product-Manual DaVis 8.2 Software*. 8th Ed. Göttingen, Germany.

LaVision GmbH (2015). *StrainMaster Advanced Digital Image Correlation Systems for Optical Full Field Measurement of Material Strain, Displacement and Shape*. Göttingen, Germany.

Lecompte, D., Smits, A., Bossuyt, S., Sol, H., Vantomme, J., Van Hemelrijck, D. and Habraken, A.M. (2006). Quality assessment of speckle patterns for digital image correlation. *Optics and Lasers in Engineering*, vol. 44, no. 11, pp. 1132–1145.

Lefik, M. and Schrefler, B. (2003). Artificial neural network as an incremental non-linear constitutive model for a finite element code. *Computer Methods in Applied Mechanics and Engineering*, vol. 192, no. 28-30, pp. 3265–3283.

Li, S., Zhou, C., Yu, H. and Li, L. (2011). Formulation of a unit cell of a reduced size for plain weave textile composites. *Computational Materials Science*, vol. 50, no. 5, pp. 1770–1780.

Lin, H., Clifford, M., Long, A. and Sherburn, M. (2008). Finite element modelling of fabric shear. *Modelling and Simulation in Materials Science and Engineering*, vol. 17, no. 1.

Liu, L., Chen, J., Li, X. and Sherwood, J. (2005). Two-dimensional macro-mechanics shear models of woven fabrics. *Composites Part A: Applied Science and Manufacturing*, vol. 36, pp. 105–114.

Lomov, S., Huysmans, G., Luo, Y., Parnas, R., Prodromou, A., Verpoest, I. and Phelan, F. (2001). Textile composites: modelling strategies. *Composites Part A: Applied Science and Manufacturing*, vol. 32, no. 10, pp. 1379–1394.

Lomov, S., Ivanov, D., Verpoest, I., Zako, M., Kurashiki, T., Nakai, H. and Hirosawa, S. (2007). Meso-FE modelling of textile composites: Road map, data flow and algorithms. *Composites Science and Technology*, vol. 67, no. 9, pp. 1870–1891.

Pan, N. (1996). Analysis of woven fabric strengths: Prediction of fabric strength under uniaxial and biaxial extensions. *Composites Science and Technology*, vol. 56, no. 3, pp. 311–327.

Parsons, E., Weerasooriya, T., Sarva, S. and Socrate, S. (2010). Impact of woven fabric: Experiments and mesostructure-based continuum-level simulations. *Journal of the Mechanics and Physics of Solids*, vol. 58, no. 11, pp. 1995–2021.

Peirce, F. (1937). The geometry of cloth structure. *The Journal of The Textile Institute*, vol. 28, p. 4596.

Peng, X. and Cao, J. (2002). A dual homogenization and finite element approach for material characterization of textile composites. *Composites Part B: Engineering*, vol. 33, no. 1, pp. 45–56.

Peng, X. and Cao, J. (2005). A continuum mechanics-based non-orthogonal constitutive model for woven composite fabrics. *Composites Part A: Applied Science and Manufacturing*, vol. 36, pp. 859–874.

Potluri, P. and Thammandra, V. (2007). Influence of uniaxial and biaxial tension on meso-scale geometry and strain fields in a woven composite. *Composite Structures*, vol. 77, no. 3, pp. 405–418.

Sagar, T., Potluri, P. and Hearle, J. (2003). Mesoscale modelling of interlaced fibre assemblies using energy method. *Computational Materials Science*, vol. 28, pp. 49–62.

Shahkarami, A. and Vaziri, R. (2007). A continuum shell finite element model for impact simulation of woven fabrics. *International Journal of Impact Engineering*, vol. 34, no. 1, pp. 104–119.

Tan, P., Tong, L. and Steven, G. (1997). Modelling for predicting the mechanical properties of textile compositesA review. *Composites Part A: Applied Science and Manufacturing*, vol. 28, no. 11, pp. 903–922.

Venter, M.P. (2015). *A Methodology for Numerical Prototyping of Inflatable Dunnage Bags*. PhD Dissertation, Stellenbosch University.

Verpoest, I. and Lomov, S. (2005). Virtual textile composites software : Integration with micro-mechanical, permeability and structural analysis. *Composites Science and Technology*, vol. 65, no. 15-16, pp. 2563–2574.

Yun, G.J., Ghaboussi, J. and Elnashai, A.S. (2007). A new neural network-based model for hysteretic behavior of materials. *International Journal for Numerical Methods in Engineering*, vol. 73, pp. 447–469.